

Fluorescence Sensing of Inorganic Phosphate and Pyrophosphate Using Small Molecular Sensors and Their Applications

Jirarut Wongkongkatap¹ · Akio Ojida² · Itaru Hamachi³

Received: 28 October 2016 / Accepted: 1 February 2017 / Published online: 1 March 2017
© Springer International Publishing Switzerland 2017

Abstract The aim of this contribution is to provide an introduction and a brief summary of the principle of fluorescence molecular sensors specific to inorganic phosphate (Pi) and inorganic pyrophosphate (PPi) as well as their applications. In our introduction we describe the impact of both Pi and PPi in the living organism and in the environment, followed by a description of the principle of fluorescence molecular sensors and the sensing mechanism in solution. We then focus on exciting research which has emerged in recent years on the development of fluorescent sensors specific to Pi and PPi, categorized by chemical interactions between the sensor and the target molecule, such as hydrogen bonding, coordination chemistry, displacement assay, aggregation induced emission or quenching, and chemical reactions.

This article is part of the Topical Collection “Phosphate Labeling and Sensing in Chemical Biology”; edited by Henning Jessen.

✉ Itaru Hamachi
ihamachi@sbchem.kyoto-u.ac.jp

Jirarut Wongkongkatap
jirarut.chu@mahidol.ac.th

Akio Ojida
ojida@phar.kyushu-u.ac.jp

¹ Department of Biotechnology, Faculty of Science, Mahidol University, 272 Rama 6 Road, Bangkok 10400, Thailand

² Graduate School of Pharmaceutical Sciences, Kyushu University, 3-1-1 Maidashi, Higashi-ku, Fukuoka 812-8582, Japan

³ Department of Synthetic Chemistry and Biological Chemistry, Graduate School of Engineering, Kyoto University, Katsura, Nishikyo-ku, Kyoto 615-8510, Japan

Keywords Fluorescence detection · Molecular sensor · Phosphate · Pyrophosphate · Imaging

1 Introduction

Phosphates play a central role in the building of the most fundamental molecules in living organisms, such as DNA and RNA. Along with proteins and carbohydrates, DNA and RNA constitute the three major macromolecules essential for all known forms of life. Phosphates are also major constituents of membrane lipids (in the form of phospholipids) and are involved in many biological processes, including skeletal development and bone integrity, energy metabolism, cell sensing, and regulation of protein synthesis [1]. Approximately 85% of total body inorganic phosphate (Pi) is found in bone, primarily in association with calcium in hydroxyapatite crystals deposited onto the collagen matrix [2]. The remainder is in soft tissue, with only approximately 1% in extracellular fluids [3]. Prolonged Pi deficiency results in hypophosphatemia with accompanying serious biological consequences, such as impaired mineralization of bone resulting in osteomalacia or rickets, dysfunction of the central nervous system, increased erythrocyte membrane rigidity, abnormal function of leukocytes and platelets, weakness of rhabdomyolysis and muscle, and cardiac dysfunction and respiratory failure [4–7]. At the other end of the spectrum, hyperphosphatemia is now recognized to decrease life expectancy and lead to seizures, cardiac dysrhythmias, chronic kidney disease, muscle weakness and tetany, decreased visual acuity, soft tissue calcification, and eventually death [8–13]. Therefore, controlling the Pi concentration is critical for the well-being of the organism.

Inorganic pyrophosphate (PPi), the dimeric form of Pi and a by-product of cellular hydrolysis of ATP, DNA polymerization, and other metabolic processes, is a biologically important target given its role in many crucial reactions [14, 15]. The difference in PPi concentrations in a variety of biological environments may be a diagnostic marker for various clinical conditions. For example, abnormally high levels of PPi in synovial fluid are observed for patients with calcium pyrophosphate crystal deposition disease [16–19]. Hence, the sensing and imaging of PPi has become an important research target. Phosphates are not only essential factors in living organisms, they are also important as components of several medicinal drugs and fertilizers. Eutrophication in the aquatic ecosystem is often related to pollution from phosphates and phosphorylated compounds [20, 21]. Due to their importance in both biological and environmental fields, great efforts have been made to develop systems capable of selectively sensing phosphates and their related compounds. Several comprehensive reviews describing the recognition of phosphate molecules by artificial receptors have been published [22–32].

Molecular sensors for phosphate anions usually consist of a Pi/PPi binding (receptor) site covalently linked to a sensing unit, such as a fluorophore (Fig. 1). One of the main difficulties in designing appropriate binding sites for Pi arises from the high hydration energy of this anion (-2765 kJ/mol) that places it near

the bottom of the Hofmeister selectivity series [33]. Moreover, most of the phosphate-type anions exist in water, at different pH, in different protonated states bearing different negative charges: H_3PO_4 , H_2PO_4^- , HPO_4^{2-} , and PO_4^{3-} . For these reasons, most of receptors prepared in early studies work only in organic solvents, and even in such examples, it has been pointed out that the binding of the Pi/PPI anions to artificial receptors requires optimization of both electrostatic and hydrogen-bond interactions through topological complementarity. One of the strategies adopted in the design of receptors for Pi/PPI useful in aqueous solution involves the usage of easily protonated polycations, such as polyammonium, imidazolium, and guanidinium moieties. An early pioneer in this area was A.W. Czarnik, who designed and synthesized fluorescent chemosensors for PPI [34]. The sensing unit can be attached to the receptor (binding unit) directly so that the receptor is part of the conjugated π system of the fluorophore, or it can be separated from the receptor via a covalent linker (Fig. 1). Pi/PPI sensing is based upon a variety of signal transduction mechanisms, such as binding-induced modulation in the fluorescence/absorbance using a conventional molecular recognition means (e.g., hydrogen bonding and coordination chemistry). In recent years, more elaborate methods of fluorescence sensing have emerged which involve a metal displacement assay in which the metal ion in the complex is specifically removed by Pi/PPI, and the aggregation induces emission/quenching upon binding to Pi/PPI. Sensors exhibiting covalent bond formation/breaking upon coupling Pi/PPI binding have also been reported.

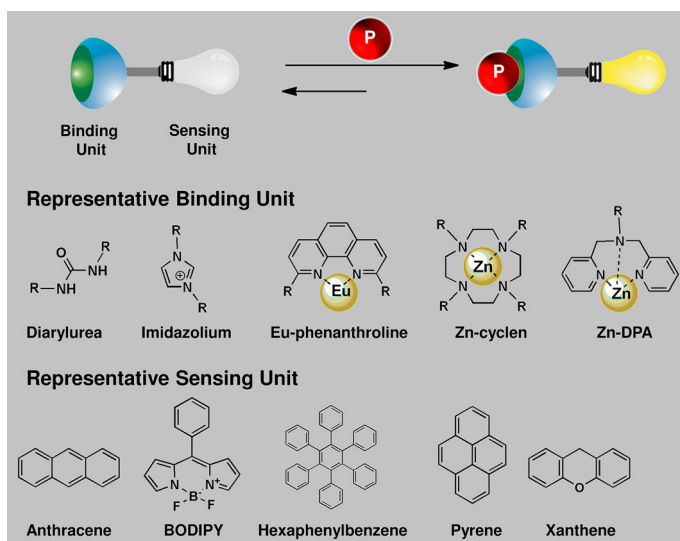


Fig. 1 Schematic overview of fluorescence sensing using a molecular sensor for phosphate (P) consisting of a binding and a sensing unit. The sensor is shown as a “Turn-ON” fluorescent sensor, but “Turn-OFF” sensors are also plausible. The chemical structures of the representative binding and sensing units are displayed

2 Molecular Sensors Based on Conventional Host–Guest Chemistry and Their Applications

Several interactions, such as electrostatic interaction, hydrogen bonds, metal ligand complexation or coordination chemistry, and hydrophobic interactions, have been employed for Pi/PPi binding, many of which are incorporated into the receptor site. From the viewpoint of the development of sensing systems in the last decade, the majority of the chemosensors for phosphate anions are rationally conjugated to an appropriate sensing unit, so that the binding events can be experimentally measured by spectroscopic changes resulting from excimer formation [35–39], intramolecular charge transfer processes (ICT) [40, 41], metal-to-ligand charge transfer processes (MLCT) [42] or photo-induced electron transfer processes (PET) [43, 44]. Receptor design still remains challenging, in particular for efficient sensing toward the complicated phosphate derivatives or the related biological events with high selectivity and sensitivity in aqueous solutions. Monitoring events over an appropriate time is also critical.

2.1 Hydrogen Bonding

The hydrogen bond is an attractive interaction between a hydrogen atom from a molecule or a molecular fragment X–H, in which X is more electronegative than H, and an atom or a group of atoms in the same or a different molecule, in which there is evidence of bond formation [45]. Common hydrogen bond donors generally used as a receptor for phosphates include amide, ammonium, imidazolium, guanidinium, pyridinium, and urea. The strength of the hydrogen bond is generally determined by electrostatic interaction, which is typically stronger than van der Waals force but weaker than the covalent or ionic bond. Therefore, most receptors contain multiple hydrogen bond donors that are carefully designed to provide a preorganized binding unit suitable for several different anions, including Pi/PPi (Fig. 2). Unfortunately, these receptors do not work well in aqueous solution, only showing an excellent sensing capability in pure organic solvent or an aqueous/organic solvent mixture because in organic solvent, the solvation energy is not that strong and supramolecular interactions play a more important role.

2.1.1 Pi Sensing

Kumar and Srivastava [38] reported a protonated sensor built on a pyridine-2,6-bis-carboxamide framework as a binding unit and pyrene as fluorophore **1** (Table 1). This system showed a blue fluorescence corresponding to the pyrene monomer and a green fluorescence resulting from pyrene excimer upon the addition of NaH₂PO₄ or NaHSO₄ in CH₃CN. In the presence of perylene monoimide-based red emitter (PMI) and in response to the addition of these oxyanions, the sensor gave rise to white light emission visible to the human eye due to the panchromatic emission. UV/Vis and ¹H-nuclear magnetic resonance (NMR) spectroscopy studies suggested the involvement of hydrogen bonding in addition to electrostatic interactions in the

stabilization of the anion–sensor complex [38]. Because no evidence of energy transfer between the pyrene and PMI was found, the emission perceived as white light is simply a composite emission of the two fluorophores emitting independently.

A selective detection of H_2PO_4^- in CH_3CN by a complete Turn-OFF fluorescence emission with tetraamide-based receptors bearing quinolyl moieties (**2**; Table 1) was investigated in 2013 by Kondo and Takai [46]. Similar but less significant fluorescence and UV–Vis changes of sensor **2** were recorded upon the addition of CH_3COO^- , HSO_4^- , and Cl^- . The results of the UV–Vis and fluorescence titrations of sensor **2** imply that the nitrogen atoms of the quinolyl groups play a crucial role in the discrimination between H_2PO_4^- and CH_3COO^- because they act as hydrogen bond acceptors for hydroxy groups of H_2PO_4^- while four amide NH groups act as hydrogen bond donors to recognize anionic oxygen atoms of H_2PO_4^- and CH_3COO^- . The high selectivity of H_2PO_4^- over CH_3COO^- was achieved because CH_3COO^- cannot form such hydrogen bonds due to the lack of a hydroxy group in CH_3COO^- . The fluorescence quenching induced by the association with H_2PO_4^- over CH_3COO^- could be attributed to PET.

A series of macrocyclic sensors based on benzimidazolium and urea appended with acridine **3** (Table 1) for ratiometric sensing of H_2PO_4^- were reported in 2013 by Martinez and Gao [47]. Adding 3.0 eq. of H_2PO_4^- tetrabutyl ammonium salt to the solution of sensor **3** resulted in quenching of fluorescence by 68% at 430 nm and enhancement of fluorescence by 4.3-fold at 501 nm, which could be attributed to the anion-induced acridine excimer, resulting in the fluorescent color change from blue (430 nm) to green (501 nm) (Fig. 3). However, HSO_4^- was able to give rise to the excimer peak of the acridine derivative **3** at 501 nm. Ratiometric sensing seems to be a versatile principle for the class of benzimidazolium–urea-based receptors, showing that they could be used as ratiometric fluorescent sensors for H_2PO_4^- via the mechanism of anion-induced fluorophore dimer formation [47, 48].

Luis, Vila, and coworkers [49] investigated an acridine-based pseudopeptidic receptor which showed a high fluorescence Turn-ON specific to H_2PO_4^- in CHCl_3 . The macrocyclic **4** (Table 1) was found to display an increase of fluorescence emission corresponding to a new band centered at 510 nm, whereas the original fluorescence at 420 nm disappeared in the presence of H_3PO_4 . The response toward other anions was practicably negligible. As already mentioned, the solvent has an important effect on the recognition process. In water, the solvation energy is larger

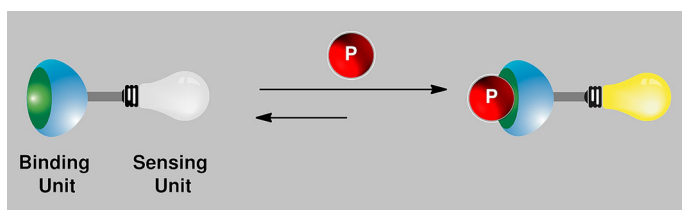
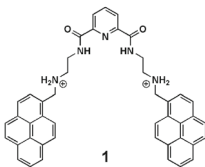
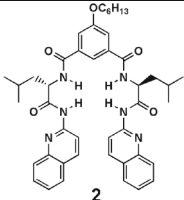
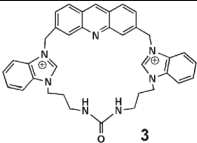
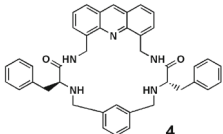
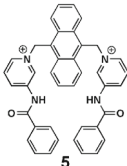


Fig. 2 Schematic overview of the fluorescent sensors utilizing hydrogen bonding for specific binding with phosphates (P)

Table 1 Inorganic phosphate sensors based on hydrogen bonding interactions

Chemical structures	Fluorescence sensing properties Proposed sensing mechanism	Binding stoichiometry (Sensor:Pi)	Binding constant (Solvent system)	Applications	Ref.
 1	Emission ON (~ 35-fold at 480 nm) $\lambda_{ex} = 344$ nm Excimer formation	1:1	$6 \times 10^4 \text{ M}^{-1}$ (CH ₃ CN) ($1.2 \times 10^5 \text{ M}^{-1}$ for sulfate anion)	NA	[38]
 2	Emission OFF (nearly perfect quenching at 355 nm) $\lambda_{ex} = 318$ nm PET	1:1	$2.76 \times 10^6 \text{ M}^{-1}$ (CH ₃ CN)	NA	[46]
 3	Ratiometric emission red-shift ($F_{430 \text{ nm}}/F_{501 \text{ nm}}$) $\lambda_{ex} = 357$ nm Excimer formation	1:1	$2.9 \times 10^6 \text{ M}^{-1}$ (CH ₃ CN)	NA	[47]
 4	Emission ON (~ 120-fold at 510 nm) $\lambda_{ex} = 357$ nm Formation of acridinium cation	NA	NA (CHCl ₃)	NA	[49]
 5	Emission ON (~ 100-fold at 500 nm) $\lambda_{ex} = 360$ nm Excimer formation	2:2	$3.0 \times 10^6 \text{ M}^{-1}$ (CH ₃ CN)	NA	[50]

NA not available

than the host–guest binding energy. Thus, spectra from titrations in water show an isosbestic point which results from an equilibrium observed between the triprotonated and the diprotonated receptor, and no supramolecular species are detected. In contrast, in chloroform, solvation energy is not as important, and supramolecular interactions play an important role. The behavior of compounds of **4** in acidic

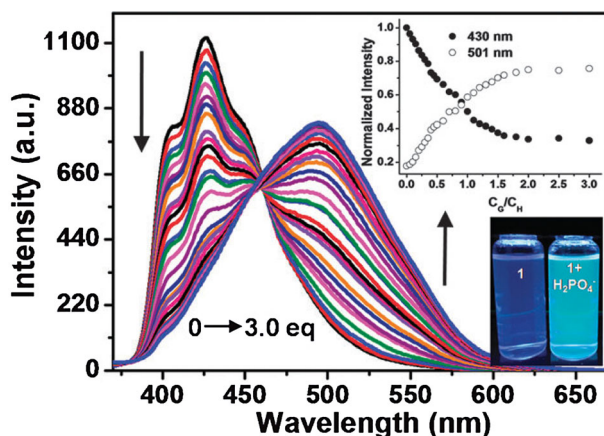


Fig. 3 Fluorescence titrations of 5×10^{-6} M sensor **3** (Table 1) excited at 357 nm with H_2PO_4^- in CH_3CN . *Insets:* *Top* Normalized emission developments at the wavelength of monomer and excimer peaks as a function of H_2PO_4^- equivalents, *bottom* fluorescent color of sensor **3** in the absence or presence of H_2PO_4^- under a UV lamp excited at 365 nm. Reproduced from Zhang et al. [47] with permission from The Royal Society of Chemistry

medium is comparable to the that shown by acridine in this study. Therefore, it can be concluded that the fluorescent moiety in the supramolecular complex formed between **4** and H_2PO_4^- in CHCl_3 is always the acridinium fluorophore, which was confirmed experimentally via fluorescence pH titrations, fluorescence lifetime, $^1\text{H-NMR}$, and X-ray studies as well as by computational calculations.

A selective sensing of H_2PO_4^- in CH_3CN driven by the assembly of anthryl amidopyridinium ligand **5** (Table 1) was demonstrated by Gong, Ning, and coworkers [50]. The ligand **5** showed a relatively low fluorescence intensity, which was ascribed to the quenching effect of a PET process from the anthracene moieties to the charged pyridinium ring. With an increase in the concentration of **5** in CH_3CN from 10^{-5} to 10^{-4} M, a new excimer emission peak centered at 539 nm was observed, which might be due to the relative proximity of the anthracene moiety at higher concentrations. This result indicated that **5** has a tendency to aggregate to some extent at high concentration. Upon the addition of various inorganic anions, including Pi, to the ligand solution, the anthryl group of **5** exhibited a strong excimer emission via H_2PO_4^- -directed assembly, while other anions showed a negligible effect. The Job plot and elemental analysis confirmed the 1:1 stoichiometry for the **5**-Pi complex. Considering there is only one anthracene fluorophore in the **5** structure and the appearance of the excimer emission between anthracene fluorophores upon addition of Pi, a plausible 2:2 stoichiometry between **5** and H_2PO_4^- was proposed, supported by absorption spectra and density functional theory (DFT) calculation [50].

2.1.2 PPI Sensing

Caltagirone et al. reported fluorescent symmetric bis-ureas [51] and asymmetric bis-urea receptor **6** [52], as shown in Table 2 for PPI recognition in dimethyl sulfoxide (DMSO) and in pure water once embedded in cationic surfactant cetyltrimethylammonium bromide (CTAB) micelles. A strong interaction between PPI and **6** was observed by $^1\text{H-NMR}$, and a 1:1 receptor/anion molar ratio of the adduct in the solid state was confirmed by crystallography of the analog of **6** and $\text{H}_2\text{PPI}^{2-}$. Upon addition of PPI, the decrease in the emission band of the naphthalene fragment at 376 nm was observed to be concurrent with the formation of a new emission band centered at 476 nm. The addition of other anions, such as Pi and F^- , caused the formation of a new band at 476 nm, but its intensity was negligible compared to that observed in the case of PPI. The formation of a new red-shifted band can be attributed to a possible anion-assisted intermolecular π - π interaction involving the indole and the naphthalene groups, as suggested by theoretical calculations. Compound **6** is also able to selectively sense HPPI^{3-} in pure water by means of fluorescence quenching once embedded in CTAB micelles.

Molina et al. [53] reported a bis(carbazoly)urea bearing two pyrene fluorophores (**7**; Table 2) as a selective receptor for the recognition of PPI in anhydrous CH_3CN or $\text{CH}_3\text{CN-H}_2\text{O}$ 85/15. In anhydrous CH_3CN , **7** showed a broad and red-shifted emission band at 496 nm, assigned to the excimer emission of the pyrene moiety, and two sharp bands at 416 and 394 nm, arising from the monomer emission. The intensity ratio of excimer to monomer, $I_E/I_M = 1.06$, was barely changed in the concentration range of 10^{-7} – 10^{-5} M, indicating that the excimer emission results from an intramolecular excimer but not from an intermolecular interaction. Binding with PPI perturbs the intramolecular excimer emission of pyrene because the presence of the PPI interacting with the binding cavity forces the side chains to open in order to accommodate the guest into the cavity, thereby disabling any possibility of forming an intramolecular excimer. On the other hand, in aqueous mixture, $^1\text{H-NMR}$ and quantum chemical calculations suggest that the $7\cdot(\text{H}_2\text{O})(\text{PPI})_2$ complex displays quasi- C_2 symmetry and features all eight NH groups pointing inward to the cavity and an efficient pyrene–pyrene parallel stacking which induces an increase in excimer emission of the receptor upon binding to PPI.

2.2 Coordination Chemistry

While hydrogen bonding interactions have been widely utilized in the development of selective anion receptors and sensors in organic solvents [54], it has shown only limited success in selective anion recognition in aqueous systems [52, 53]. Because most phosphate anions and their derivatives are in water, it is crucial to bind and sense these species in aqueous medium. It is now regarded that one of the most powerful strategies for phosphate anion recognition and sensing in water is the utilization of coordination chemistry, where one or two vacant coordination sites of metal complexes are employed for binding anionic guest molecules [55–62]. In many cases, multiple metal ions are positioned on an organic scaffold at appropriate

Table 2 Inorganic pyrophosphate sensors based on hydrogen bonding interactions

Chemical structures	Fluorescence sensing properties Proposed sensing mechanism	Binding stoichiometry (Sensor:PPi)	Binding constant (Solvent system)	Applications	Ref.
 6	Ratiometric emission red-shift $(F_{476\text{ nm}}/F_{376\text{ nm}})$ $\lambda_{\text{ex}} = 328\text{ nm}$ Excimer formation	1:1	NA but experimental evidence suggests strong interaction (DMSO)	NA	[52]
	Emission OFF (~40% at 364 nm) $\lambda_{\text{ex}} = 326\text{ nm}$ NA	NA	NA	(micellar aqueous solution of cationic surfactant CTAB)	
 7	Emission OFF (~71% at 500 nm) $\lambda_{\text{ex}} = 345\text{ nm}$ Excimer deformation	1:1	$\text{Log } K_{11} = 7.00 \pm 0.57$ (anhydrous CH_3CN)	NA	[53]
	Emission ON (~3.5-fold at 500 nm) $\lambda_{\text{ex}} = 345\text{ nm}$ Excimer formation	1:2	$\text{Log } \beta_{12} = 13.60 \pm 0.63$ (CH_3CN -water 85/15 v/v)		

λ_{ex} excitation wavelength, NA not available

distances to allow an anion guest to bridge the metal centers, providing a means of introducing selectivity for a specific guest (Fig. 4).

While a number of metal ions have been used in such receptors, including those of the main group, transition metals, and lanthanides, Zn^{2+} is among the most commonly employed, particularly where the guests are phosphate derivatives [28]. Kimura and his group were the first to demonstrate that the macrocyclic Zn^{2+} complex exhibits excellent binding affinities to phosphate anions and the derivatives [63, 64], inspired by the binding sites of metalloenzymes, in which phosphates act as substrates or inhibitors by reversibly coordinating to one or more Zn^{2+} ions in the active site [65]. More recently, Hamachi and his group [43, 44] proposed the Zn^{2+} -dipicolylamine (DPA) complex as a versatile binding motif for phosphate anions in water and biological fluids. The DPA is a tridentate ligand comprised of three nitrogen donors that provides good selectivity toward Zn^{2+} over other biologically relevant metal ions and leaves coordination sites free for Pi/PPi binding. One of the advantages of the Zn–DPA receptor is its simplicity in terms of synthesis and easy modification for optimization of sensor design. Subsequent to the studies of Hamachi et al. [43, 44], many types of Zn–DPA-based molecular/supramolecular sensors have been reported [28].

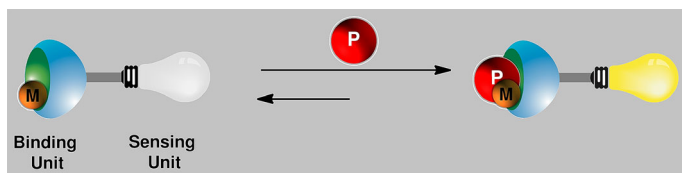


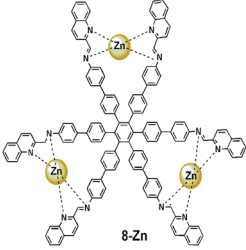
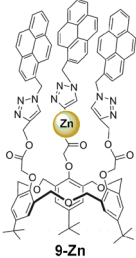
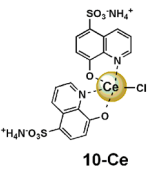

Fig. 4 Schematic overview of the fluorescent sensors utilizing coordination chemistry for the specific binding toward phosphate (*P*). *M* Metal

2.2.1 *Pi* Sensing

Bhalla, Kumar, and coworkers [55] reported the recognition of AMP and H_2PO_4^- in ethanol–tetrahydrofuran (THF; 3/1) using a Zn ensemble of a unique propeller-shaped hexaphenylbenzene derivative appended with quinoline moieties **8** (Table 3). By itself, sensor **8** does not exhibit any fluorescence emission in ethanol-THF (3/1) due to PET from imino nitrogen to a photoexcited hexaphenylbenzene moiety [66]. Upon addition of increasing amounts of Zn^{2+} ions (0–20 eq.) a strong fluorescence emission band appeared at 438 nm. This fluorescence emission band is attributed to the interaction between Zn^{2+} ions and imino nitrogens and the nitrogen atoms of the quinoline moieties as a result of which the PET is suppressed, resulting into fluorescence enhancement. Upon the addition of H_2PO_4^- between 0 and 6 eq. the emission band at 438 nm was drastically quenched, but continued addition of Pi to 6–12 eq. resulted in an increase in a new blue-shifted band at 366 nm. This result indicates the weakening of the existing **8**–Zn bond due to the interaction of H_2PO_4^- with Zn. On the other hand, the addition of AMP led to the enhancement of emission intensity along with a slight blue shift in the signal from 438 to 431 nm while no significant fluorescence change was observed upon addition of other anions. A multichannel molecular keypad system based on three different chemical inputs (Zn^{2+} , H_2PO_4^- , AMP) that switches between two different fluorescent outputs at 431 and 366 nm has been successfully constructed [55].

Yamato and collaborators [56] investigated a pyrenyl-linked triazole-modified homooxacalix [3] arene based ratiometric fluorescent receptors **9** selective for H_2PO_4^- ions (Table 3). This system exhibited a cascade signal output for the ligand toward Zn^{2+} and consequently H_2PO_4^- through switching of the excimer/monomer emission of pyrene at 485/396 nm from the “ON–OFF” to the “OFF–ON” type. The smaller downfield chemical shift of triazole proton suggests that the Zn^{2+} ion of complex **9** may be located in the negative cavity formed by the nitrogen-rich triazole ligand and the carbonyl group. In particular, the coordination force of the Zn^{2+} ion would prevent the three pyrene moieties from maintaining π – π stacking for the excimer emission and instead leads to a concomitant increase of the monomer emission of the pyrene in the fluorescence spectra. $^1\text{H-NMR}$ results suggested that the receptor **9** and the H_2PO_4^- anion not only have strong coordination and electrostatic interactions but also have strong hydrogen bonding interactions. As a result, the ratiometric signal of I_{485}/I_{396} of complex **9** changes from the OFF to the ON state upon addition of the H_2PO_4^- ion. A design of

Table 3 Inorganic phosphate sensors based on coordination chemistry

Chemical structures	Fluorescence sensing properties Proposed sensing mechanism	Binding stoichiometry (Sensor:Pi)	Binding constant (Solvent system)	Applications	Ref.
 8-Zn	Emission OFF (~90% at 438 nm) λ_{ex} = 287 nm PET	NA	NA (EtOH-THF, 3/1 v/v)	Potential bioprobe and multichannel keypad system	[55]
 9-Zn	Ratiometric emission red-shift ($F_{485\text{ nm}}/F_{395\text{ nm}}$) λ_{ex} = 343 nm Excimer formation	1:1	$1.01 \times 10^5 \text{ M}^{-1}$ (CH ₃ CN-CH ₂ -Cl ₂ -H ₂ O, 1000/1/5 v/v)	Potential molecular traffic signal with an R-S latch logic circuit	[56]
 10-Ce	Emission ON (~2-fold at 496 nm) λ_{ex} = 460 nm ICT	1:1	$3.0 \times 10^6 \text{ M}^{-1}$ (aqueous solution, pH 8)	Analysis of Pi content in fertilizer and tap water	[59]
 11-Ln	Eu complex Emission OFF (~95% at 618 nm) λ_{ex} = 276 nm NA	1:1	$\text{Log } K_b = 5.4 \pm 0.01$ (10 mM HEPES, pH 7.4)	Staining of microalgal cell (<i>Chlorella vulgaris</i> CCNM 1017)	[60]
	Tb complex Emission OFF (~98% at 543 nm) λ_{ex} = 278 nm NA	1:1	$\text{Log } K_b = 5.5 \pm 0.01$ (10 mM HEPES, pH 7.4)		

λ_{ex} , excitation wavelength, NA not available

molecular logic gate using Zn^{2+} and H_2PO_4^- ions as the chemical inputs and the fluorescence emission at 396 and 485 nm as an output signal was also reported [56].

Ganjali et al. [59] reported a bis(8-hydroxy quinoline-5-sulphonate) cerium(III) complex **10-Ce** as a novel fluorescence Turn-ON sensor specific for Pi recognition

(Table 3). The significant fluorescence enhancement might be a result of the electrostatic interaction between Pi and the **10**-Ce complex, in which two oxygen atoms of the Pi bridge interact with the center of Ce^{3+} to reduce the magnitude of the electron withdrawal via partial neutralization of the charge on the Ce^{3+} ion, thereby increasing the electron-donating character of the quinolone-5-sulphonate moiety and finally resulting in an increased efficiency of ICT [67].

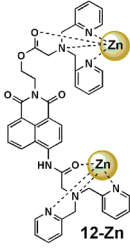
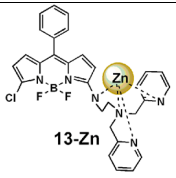
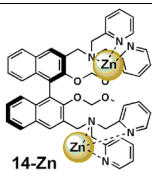
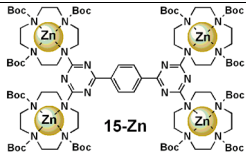
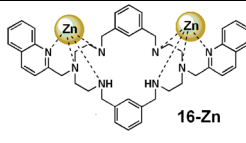
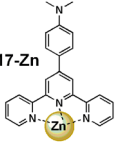
The lanthanide (III) complex of bis-amine-substituted phenanthroline-based chiral ligand (**11**; Table 3) was subsequently synthesized and characterized in 2014 by Subramaniam, Mishra, Albrecht and their coworkers [60]. Although water is known to be a quencher of lanthanide complexes, both complexes show intense luminescence in HEPES buffer (10 mM, pH 7.4), which is attributable to a $J = 2$ transition (${}^5D_0 \rightarrow {}^7F_2$) [68]. Complexes **11**-Eu and **11**-Tb show red and green emission, which displayed a selective sensing of Pi through 95 and 98% fluorescence quenching over other anions such as CH_3COO^- , NO_3^- , and SO_4^{2-} . A strong fluorescence quenching was also observed in the case of NO_2^- , ATP, ADP, and AMP. The same selectivity was observed in the case of the bis-imine-substituted phenanthroline-based Eu complex reported previously [58]. Both complexes were shown to be useable as a cell-staining reagent to monitor phosphates present in biological membranes, as demonstrated in the case of the green microalga (*Chlorella vulgaris* CCNM 1017).

2.2.2 PPI Sensing

Kim and co-workers [69] reported a 1,8-naphthalimide-DPA-Zn (II) complex **12**-Zn (Table 4) as a PPI-selective fluorescence Turn-OFF probe. The sensor **12**-Zn exhibits significant fluorescence quenching upon binding to both PPI (approx. 52%) and ATP (approx. 31%) over other anions in 95% aqueous solution containing CH_3CN . However, the binding of PPI induced a blue shift (approx. 23 nm), while a blue shift was not observed in the case of ATP. In contrast to the bis[DPA-Zn(II)] complexes discussed in other reports [70–72], where binding to PPI generally involved two Zn(II) ions, time-dependent DFT calculations at the level of B3LYP/6-31G (d) suggests that only one of the DPA-Zn(II) centers in **12**-Zn binds directly to PPI. However, no experimental data to support the proposed binding mode between **12**-Zn-PPI complex was provided in the study [69]. Molecular orbital studies predict that available electron density in either of the chelating moieties may participate in PET, which causes fluorescence quenching in the ligand. Binding of Zn^{2+} with chelating moieties eliminates the available electron density from the chelating moieties in **12** and, therefore, PET is not possible in the **12**-Zn complex. Upon binding with PPI, the photo-induced charge transfer occurs from negatively charged PPI to either the DPA unit or a fluorophore moiety. A biological application was also attempted, namely, to monitor intracellular PPI by addition of **12**-Zn to C2C12 cells with exogenous PPI.

Wu et al. [70] demonstrated a PPI selective BODIPY-based fluorescence probe **13**-Zn complex (Table 4) and its imaging in a living RAW264.7 cell line. Fluorescence quenching with 10-nm blue shift was observed upon the addition of PPI, whereas the other anions, including nucleoside polyphosphate (NPP), caused

Table 4 Inorganic pyrophosphate sensors based on coordination chemistry

Chemical structures	Fluorescence sensing properties Proposed sensing mechanism	Binding stoichiometry (Sensor:PPi)	Binding constant (Solvent system)	Applications	Ref.
 12-Zn	Emission OFF (~ 52% at 504 nm) λ_{ex} = 360 nm PET/PCT	NA	NA (CH ₃ CN-20 mM HEPES, pH 7.4, 5/95 v/v)	Fluorescence imaging using C2C12 cells with 500 and 1000 eq. exogenous PPi.	[69]
 13-Zn	Emission OFF (~ 72% at 549 nm) λ_{ex} = 465 nm NA	1 : 1	$6.9 \times 10^4 \text{ M}^{-1}$ (CH ₃ OH-5 mM HEPES, pH 7, 1/49 v/v)	Fluorescence imaging using RAW264.7 cells with Zn ²⁺ followed by 1 eq. exogenous PPi	[70]
 14-Zn	Emission ON (~ 4-fold at 383 nm) λ_{ex} = 316 nm PET	1:1	$6.7 \times 10^3 \text{ M}^{-1}$ (CH ₃ OH-10 mM HEPES, pH 7.4, 1/99 v/v)	Fluorescence imaging using HeLa cells with 2 eq. exogenous PPi	[71]
 15-Zn	Emission OFF (~ 90% at 385 nm) λ_{ex} = 290 nm Dimer formation	1:2	$> 10^6 \text{ M}^{-1}$ (25 mM HEPES, pH 7.4)	NA	[73]
 16-Zn	Emission ON (~ 21-fold at 368 nm) λ_{ex} = 302 nm ESICT	NA	6.22 log unit (20 mM MOPS, pH 7.4)	NA	[74]
 17-Zn	Emission ON (~ 500-fold at 591 nm) λ_{ex} = 440 nm NA	3:1	NA (10 mM HEPES, pH 7.4)	Fluorescence imaging of HeLa cells without addition of exogenous PPi. Hydrogel coated paper strips for PPi	[75]

 λ_{ex} excitation wavelength, NA not available

only minor fluorescence quenching or even induced a slight increase in fluorescence emission in a water–methanol mixture. $^1\text{H-NMR}$ spectroscopy and DFT calculation suggested that Zn^{2+} binding occurs mainly through the four nitrogens at the *N,N*-di(pyridin-2-ylmethyl)-ethane-1,2-diamine substituent and confirmed the binding of PPI with the **13**–Zn complex. These observations indicate that PPI binding to the Zn^{2+} results in weaker binding between **13** and Zn^{2+} . Living cell imaging using the RAW264.7 cell line showed that the green fluorescence of the BODIPY-based **13**–Zn complex disappeared when 1 eq. of PPI was applied.

The Zn complex of 1,1'-bi-2-naphthol bearing DPA units **14** (Table 4) that make PPI visible was investigated by Li, Yu, and their coworkers [71]. A fluorescence enhancement of **14** at 383 nm in 1% methanol/HEPES buffer was observed upon the addition of Zn^{2+} due to the suppression of PET from the lone pair of electrons on the DPA group. The fluorescence of the **14**–Zn complex was subsequently increased by approximately fourfold with the addition of PPI, wherein the intensity was saturated at 0.3 eq. Among the other anions tested, ATP was found to also enhance the fluorescence of **14**–Zn, and the selectivity coefficient for PPI and ATP was calculated to be 4.1/2.8, suggesting that the enhancement is dependent on both the bulkiness of the organic moiety and the number of phosphates. When the concentration of the **14**–Zn complex was raised from 1.0×10^{-5} to 2.5×10^{-3} M it was possible to detect the recognition of anions by the naked eye through precipitation formation. The formation of small particles (0.8–1.3 μm), observed by scanning electron microscopy (SEM), indicated that **14** was uniformly dispersed in the solution, due to its poor solubility in the HEPES solution, but that upon the addition of Zn^{2+} to the system, the solution became clear and no small particles (turbidity) were observed. Once PPI was added, rough and scaly solids with large surfaces were observed which confirmed the interaction between the **14**–Zn complex and PPI. The fluorescence imaging was demonstrated in HeLa cells treated with **14**, followed by Zn^{2+} /pyrithione and PPI.

König and Hamachi's group [73] reported a rigid luminescent bis-Zn(II)-bis-cyclen complex **15**–Zn specific for PPI (Table 4) in a completely aqueous solution. **15**–Zn displayed a strong fluorescence quenching which could arise from a similar dimerization resulting in π – π stacking interactions of planar benzene–triazine moieties. Electrospray ionization mass spectrometry (ESI-MS) measurement of the complex in the presence of an excess amount of PPI showed that the major species for the complex corresponded to the receptor/PPI = 1:2 complex, and the presence of a dimer of the complex **15**–Zn with PPI was clearly observed, enabling the isotope distribution to be compared with the predicted one.

Mateus, Delgado, and their coworkers [74] investigated a Zn complex of diethylenetriamine-derived macrocycle **16**–Zn, bearing 2-methylquinoline arms and containing *m*-xylyl spacers (Table 4). At pH 7.4, the ligand exhibits almost no fluorescence emission. Single-crystal X-ray diffraction studies indicated that the ligand is bound to each Zn center by three nitrogen atoms of a diethylenetriamine subunit and a quinolyl nitrogen atom, and the metal coordination sphere is completed by the binding of oxygen atoms of carbonate anions. Upon the addition of 1 eq. of PPI to **16**–Zn, a remarkable 21-fold enhancement of the fluorescence intensity at 368 nm was observed. The increase in fluorescence quantum yield of the

complex can be attributed to a significant increase of the radiative decay constant of the complexed quinoline fluorophore. Further addition of PPI caused a decrease in fluorescence intensity, which may be ascribed to the removal of Zn^{2+} from the complex by the PPI anion. No further fluorescence change was observed in the presence of 1 eq. of the other anions studied, including Pi, NPPs, and phenyl phosphate, indicating that the **16**-Zn receptor acts as a selective fluorescent sensor for PPI which leads to an important effect on excited-state intramolecular charge transfer (ESICT) in the quinoline ring. The selectivity of the **16**-Zn complex is most likely related to a steric hindrance effect caused by the bulky quinoline pendant arms.

In 2014 a long wavelength detection of PPI using a simple terpyridine- Zn^{2+} complex **17**-Zn (Table 4) was reported by Rissanen et al. [75]. The crystal structure of the **17**-Zn complex confirmed the formation of the 1:1 metal complex in which Zn^{2+} adopts a distorted trigonal bipyramidal N_3Cl_2 coordination. The **17**-Zn complex demonstrated an extraordinary sensitivity because the probe was able to detect PPI at nanomolar level with the lowest limit of detection of 0.8 nM, while the sensitivity of the other probes was invariably limited to micromolar levels. Although the unusual binding stoichiometry of 1:3 (PPI: **17**-Zn) was confirmed unambiguously by a Job plot analysis and the binding constant of the **17**-Zn and PPI was not available, a bright orange-yellow emission of **17**-Zn-PPI was imaged in a single HeLa cell due to the excellent sensitivity of the receptor. Almost the entire cell could be mapped for PPI, even regions with minimal PPI concentrations (Fig. 5). The maximum emission intensities were recorded at the nuclei, and emissions were also observed from the membranous cytoplasmic structures. The receptor is highly suitable for monitoring the biological events occurring in a single cell.

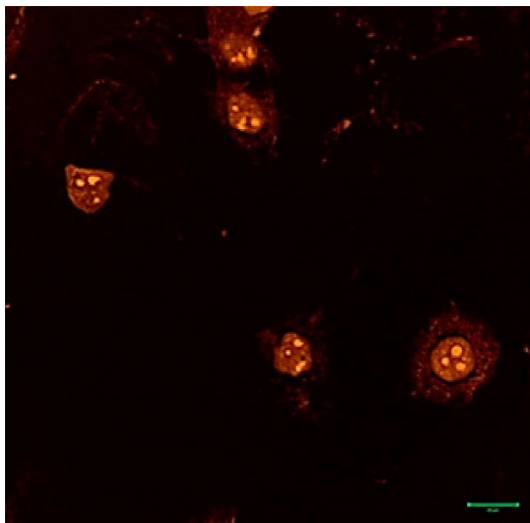
3 Molecular Sensors Based on New Sensing Mechanisms and Their Applications

Recently, several alternative approaches to Pi/PPI sensing involving metal displacement, aggregation-induced emission or quenching, and chemical reactions have emerged as simple and convenient techniques with high sensitivity. In contrast to sensing based on supramolecular chemistry such as hydrogen bonding or coordination chemistry, when the maximum fluorescence change can be recorded with a time resolution in the order of seconds, the kinetics of reaction/displacement assay-based sensing strongly depends on the nature of reaction, which is several seconds in some cases [76] while in other cases it can be very slow and more than 1 h is required to reach the highest fluorescence change [77].

3.1 Displacement Assay

In this approach, a specific metal complex is designed such that Pi/PPI has a stronger affinity for the metal ion, resulting in displacement of the metal upon Pi/PPI binding which induces a change in fluorescence (Fig. 6). Most of the metal displacement sensors demonstrate a good reversibility because the addition of the

Fig. 5 Confocal fluorescence microscopy image of HeLa cells incubated with probe **17**-Zn (50 μ M). Reprinted with permission from Bhowmik et al. [75]. Copyright 2014 American Chemical Society



metal ion can reverse the process of sensing. Another approach is the indicator displacement assay (IDA) in which an indicator is allowed to bind reversibly to a receptor in the first step. Pi/PPi with a strong affinity to the sensor is subsequently introduced into the system, causing the displacement of the indicator from the receptor, which in turn modulates the sensing unit (Fig. 6). IDA has become a popular method for converting almost any synthetic receptor into an optical sensor along the lines originally developed by Anslyn et al. [78, 79].

3.1.1 Pi Sensing

Meng, Zhang and their co-workers [80] investigated the fluorescein bearing 2-[(pyridin-2-yl-imino)methyl]phenol moiety **18**-Fe complex (Table 5) as a receptor for the highly selective detection of Pi in THF-HEPES buffer mixture. The fluorescence emission of the **18**-Fe³⁺ complex was completely quenched, which could be ascribed to the paramagnetic quenching effect of Fe³⁺ and/or MLCT. The ligand **18** displayed a high affinity to Fe³⁺ ($K_a = 1.40 \times 10^6 \text{ M}^{-1}$) over Cu²⁺ and other metal ions. The specific interaction between Pi and the **18**-Fe³⁺ complex led to the liberation of fluorophore **18**, and thus the fluorescence was approximately 9.6-fold recovered when 18 eq. Pi was added. The **18**-Fe³⁺ complex showed a negligible fluorescent response upon the addition of diverse anions but rather displayed reasonable performance (less than fourfold) with other polyphosphate species, including NPP and PPI. Studies on the quantitative deposition of **18** in MDA-MB-231 cells and its fluorescence “ON-OFF-ON” response in living cells were conducted using a flow cytometer. Staining of the Pi-pretreated MDA-MB-231 and U-343 MGa cells with the **18**-Fe³⁺ complex resulted in bright intracellular fluorescence images showing that **18** is able to display a fluorescence Turn-ON response to Pi in the living cells.

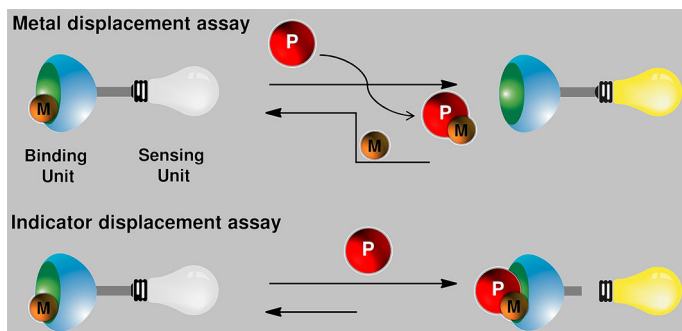


Fig. 6 Schematic overview of fluorescent sensors utilizing the metal and indicator displacement assay for the specific binding toward phosphate (*P*). *M* Metal

Table 5 Displacement assays specific to inorganic phosphate

Displacement assays	Fluorescence sensing properties Proposed sensing mechanism (solvent system)	Applications	Ref.
<p>18-Fe $\xrightleftharpoons[\text{Fe}^{3+}]{\text{Pi}}$ 18 + $\text{Fe}^{3+}\text{-Pi}$</p>	Emission ON (~ 10-fold at 515 nm) $\lambda_{\text{ex}} = 430 \text{ nm}$ Paramagnetic quenching effect of Fe^{3+} and/or MLCT (THF-20 mM HEPES, pH 7.4, 3/7 v/v)	Fluorescence imaging using MDA-MB-231 and U-343 MGA cells treated with 30/100 eq. Pi. Flow cytometry analysis of MDA-MB-231 cells treated with 30 eq. Pi	[80]
<p>19-Cu $\xrightleftharpoons[\text{Cu}^{2+}]{\text{Pi}}$ 19 + $\text{Cu}^{2+}\text{-Pi}$</p>	Emission ON (~ 4-fold at 405 nm) $\lambda_{\text{ex}} = 290 \text{ nm}$ PET (CH_3OH)	Molecular logic gate	[81]
<p>20-Zn $\xrightleftharpoons[\text{Zn}^{2+}]{\text{Pi}}$ 20 + $\text{Zn}^{2+}\text{-Pi}$</p>	Emission OFF (~ 80% at 450 nm) $\lambda_{\text{ex}} = 365 \text{ nm}$ PET (CH_3OH)	Molecular logic gate	[82]

Another report of metal displacement assay in CH_3OH was demonstrated by Hu, Ju, and their coworkers [81] in 2015. A steroid-coumarin conjugate **19** (Table 5) displayed a significant fluorescence quenching only in the presence of 9 eq. Cu^{2+}

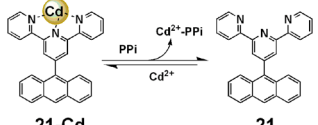
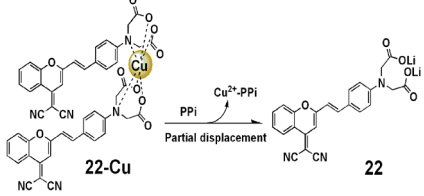
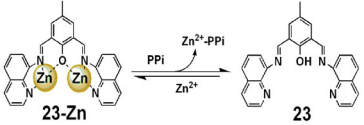
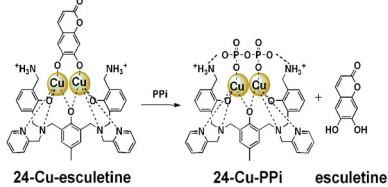
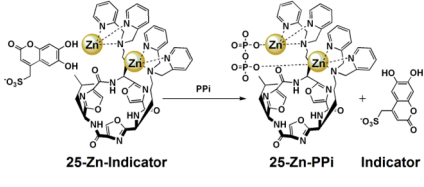
via PET resulting from the excited coumarin fluorescence in the presence of Cu^{2+} ions [67]. Furthermore, a 1:2 binding complex between the 1,2,3-triazole motif of **19** and the Cu^{2+} ion was shown using UV–Vis titration and ESI MS. When 2.0 eq. H_2PO_4^- ion was added, the absorption curve showed a dramatic change and almost reversed to the state of free compound **19**, suggesting the removal of Cu^{2+} ion from the complex by H_2PO_4^- anion. Conversely, there was no change in fluorescence in the presence of other anions, including F^- , Cl^- , Br^- , I^- , CH_3COO^- , NO_3^- , and HSO_4^- . The Turn-ON recognition ability in fluorescence for histidine was also observed as a result of the release of the free **19** after Cu^{2+} was removed from the complex to form a stable Cu–histidine complex due to the universal interaction between Cu^{2+} and amino acids. Its application as a molecular logic gate was studied with Cu^{2+} and H_2PO_4^- as input signals and the fluorescence intensity at 405 nm as output. The same research group also reported steroid–salen conjugate **20** for Zn ion recognition and cascade recognition for H_2PO_4^- in CH_3OH , showing the logic gate properties of Zn^{2+} and H_2PO_4^- [82].

3.1.2 PPI Sensing

Li, Yu, and their coworkers [83] investigated a Cd(II)-terpyridine-based complex **21**–Cd (Table 6) as a reversible ratiometric fluorescent probe for PPI detection in CH_3CN solution. The ligand has strong fluorescence emission at 421 nm, and there was a new emission peak at 553 nm upon the addition of Zn^{2+} ($I_{553}/I_{421} = 10$) or Cd^{2+} ($I_{553}/I_{421} = 30$) that did not respond to Li^+ , Na^+ , K^+ , or Ca^{2+} in CH_3CN . The red shift of the fluorescence emission of the ligand after coordination with Cd^{2+} can be ascribed to the electron-donating ability of the anthracene group, which causes ICT from the anthracene to the Cd(II)-coordinated terpyridine (see structure in Table 6). The 2:2 binding stoichiometry of the ligand and Cd^{2+} was verified by a single-crystal structure analysis and mass spectrometry. Upon the addition of PPI to the **21**–Cd complex in CH_3CN solution, the ratio of the I_{431}/I_{560} increased from 0.26 to 7.46, whereas the addition of ATP increased this ratio only from 0.26 to 2.66. The fluorescent titration, UV–Vis absorption, and high-resolution mass spectrometry results suggested that PPI could completely de-complex the **21**–Cd and liberate the ligand. This ratiometric sensing behavior of red and blue shifts upon addition of Cd^{2+} followed by the addition of PPI in fluorescence emission was reversible over five successive cycles. Finally, Li et al. [83] demonstrated the confocal fluorescence imaging of **21**–Cd complex with PPI in living RAW264.7 cells.

Zhu et al. [84] reported a near-infrared (NIR) fluorescent Turn-ON sensor **22**–Cu complex, which employs dicyanomethylene-4*H*-chromene as the fluorophore and the iminodiacetic acid group as the receptor (Table 6), for the selective detection of PPI in aqueous solution. Since α -amino acid shows a good chelating property toward Cu^{2+} [85], the incorporation of a lithium iminodiacetate group in **22** has a double effect, namely, the coordination ligand and the improvement of water solubility. There was no significant change in the fluorescence emission in the presence of other metal ions—only the addition of 5 eq. Cu^{2+} resulted in an obvious decrease in fluorescence. Job plots and mass peak analysis revealed that **22** forms a 2:1 complex with Cu^{2+} . Meanwhile, the fluorescence intensity in the NIR region of

Table 6 Displacement assay specific to inorganic pyrophosphate

Displacement assays	Fluorescence sensing properties Proposed sensing mechanism (solvent system)	Applications	Ref.
Metal displacement assay			
 <p>21-Cd $\xrightleftharpoons[\text{Cd}^{2+}]{\text{PPI}}$ 21</p>	Ratiometric emission blue-shift $(F_{431\text{ nm}}/F_{560\text{ nm}})$ $\lambda_{\text{ex}} = 326\text{ nm}$ ICT (CH ₃ CN-10 mM HEPES, pH 7.4, 1/1, v/v)	Fluorescence imaging in RAW264.7 cells treated with Cd ²⁺ followed by PPI	[83]
 <p>22-Cu $\xrightarrow{\text{PPI}}$ 22</p>	Emission ON (~4.6-fold at 675 nm) $\lambda_{\text{ex}} = 450\text{ nm}$ NA (10 mM MOPS, pH 7.0)	Fluorescence imaging of to KB cells (human nasopharyngeal epidermal carcinoma cell) supplemented with 3 eq. PPI	[84]
 <p>23-Zn $\xrightleftharpoons[\text{Zn}^{2+}]{\text{PPI}}$ 23</p>	Emission OFF (~complete quenching at 480 nm) $\lambda_{\text{ex}} = 350\text{ nm}$ ICT (CH ₃ OH-1 mM HEPES, pH 7.4, 3/2, v/v)	Molecular logic gate Detection of DNA amplification Estimation of bacterial cell numbers through PCR	[86]
Indicator displacement assay			
 <p>24-Cu-esculetine $\xrightarrow{\text{PPI}}$ 24-Cu-PPI + esculetine</p>	Emission ON (~30-fold at 465 nm) $\lambda_{\text{ex}} = 380\text{ nm}$ Association and dissociation of the indicator with 24-Cu complex (10 mM HEPES, pH 7.0)	Monitoring hydrolysis of PPI catalyzed by pyrophosphatase Detecting PPI released during PCR	[87]
 <p>25-Zn-Indicator $\xrightarrow{\text{PPI}}$ 25-Zn-PPI + Indicator</p>	Emission ON (~8-fold at 480 nm) $\lambda_{\text{ex}} = 347\text{ nm}$ Association and dissociation of the indicator with 25-Zn complex (5 mM HEPES, pH 7.4/saline solution/Krebs buffer solution)	NA	[88]

λ_{ex} excitation wavelength, NA not available

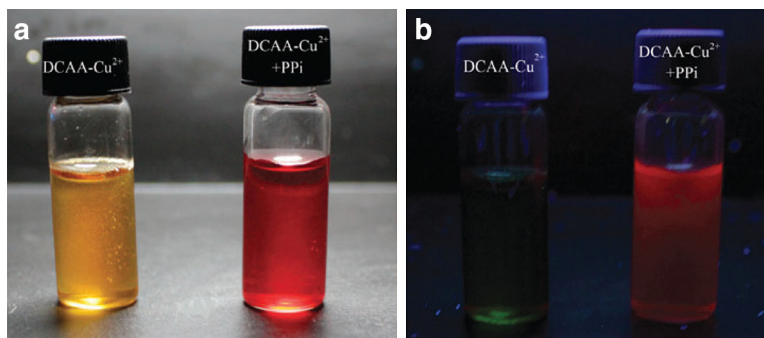


Fig. 7 Photographic images observed of the **22**–Cu complex (10^{-4} M) with the addition of inorganic pyrophosphate (PPi) at 5 eq. **a** Color change, **b** fluorescence emission change irradiated at 365 nm by a portable fluorescent lamp. Reproduced from Zhu et al. [84] with permission of The Royal Society of Chemistry

675 nm was obviously enhanced and finally stabilized upon the addition of 15 eq. of PPi. The associated color change can be easily differentiated by the naked eye (Fig. 7). Here, the fluorescence can not be recovered to the original intensity of **22**, which indirectly indicates that PPi does not form a sufficiently strong complex to completely remove Cu^{2+} from the **22**–Cu complex. To test its usefulness in a biological context, the sensor **22**–Cu was then applied to KB cells (human nasopharyngeal epidermal carcinoma cell) supplemented with 3 eq. PPi and monitored.

A diformyl–quinoline-based reversible receptor **23** (Table 6) prepared by Ramesh, Das, and coworkers [86] exhibits selective fluorometric enhancement upon the addition of Zn^{2+} in methanol aqueous solution. It is possible that the weak fluorescence of **23** is a consequence of ICT and free rotation around the azomethine ($\text{C}=\text{N}$) carbon, which brings flexibility within the ligand. In the presence of Zn^{2+} , **23**–Zn forms a rigid phenoxo-bridged binuclear Zn complex which restricts the free rotation around the azomethine carbon, thus inhibiting the ICT process, which results in enhancement of fluorescence intensity. The formation of the binuclear phenoxo-bridged metal complex **23**–Zn provides an anion binding site in each of the metal centers. The complete quenching of fluorescence was selectively observed toward PPi, while other monovalent anions and NPP showed negligible response. Job's plot and ESI–MS data revealed a 1:1 binding stoichiometry between the **23**–Zn complex and PPi, and the apparent association constant was determined to be $1.76 \times 10^4 \text{ M}^{-1}$. The change in the emission spectrum of the **23**–Zn complex upon the addition of PPi can be understood by considering the strong binding affinity of PPi toward Zn^{2+} , resulting in the release of free ligand in solution. Application of **23** as a molecular logic gate with two inputs (Zn^{2+} , PPi) and one output (emission intensity at 480 nm), and the detection of DNA amplification by PCR assay were demonstrated. The estimation of bacterial cell numbers by indirect measurement of PPi generated from the PCR reaction of the bacterial 16s rRNA universal primer was also performed in vitro.

A dinuclear-copper(II) complex **24**-Cu (Table 6) with two ammonium arms based on bis-2-[(pyridin-2-ylmethylamino)methyl]phenol as the coordinated unit was reported by Xie, Chen, and coworkers [87] in 2016. Using esculetine as a fluorescent indicator, IDA was carried out to obtain the high affinity with PPI over other anions in 10 mM HEPES buffer (pH 7.0). A fluorescence quenching of esculetine at 465 nm was observed upon the addition of 1 eq. of the **24**-Cu complex. With the addition of PPI, the fluorescence of the solution containing **24**-Cu-esculetine was recovered, indicating the liberation of esculetine from the ensemble. The ensemble of **24**-Cu-esculetine was successfully applied to monitoring the hydrolysis reaction of PPI and the released PPI from the PCR process, exhibiting its potential application in enzyme activity screening and DNA sequencing.

A family of cyclic peptide receptors bearing the DPA-Zn complex highly selective to PPI was investigated by Butler and Jolliffe [88] using indicator displacement assays in water, saline solution, and Krebs buffer. All receptors strongly bound the coumarin-based indicator, but hexapeptide scaffold receptor **25**-Zn (Table 6) had the highest affinity toward the indicator and PPI, with $\log K_a$ values of 7.3 and 9.8, respectively. The DPA-Zn unit was capable of quenching the fluorescence of the coumarin sulfonate derivative [89, 90], and the addition of 1 eq. of PPI resulted in almost complete restoration of its fluorescence intensity while the addition of ATP or ADP resulted in fourfold and 3.5-fold fluorescence enhancements, respectively. On the other hand AMP, cAMP, phosphoserine, phosphotyrosine, Pi, and the polycarboxylates acetylglutamate and Ac-Glu-Gly-Glu were not able to displace the indicator from the receptor to an appreciable extent. The enhanced selectivity of the **25**-Zn complex observed for PPI in the routinely used Krebs physiological buffer solution ensures the further development of **25**-Zn complex in a biological assay for PPI.

3.2 Aggregation Induced Emission and Quenching

Some organic molecules that are almost nonfluorescent in solution, exhibit a high capability to emit a strong fluorescence upon aggregation (Fig. 8). This exciting fluorescence phenomenon was first noted by Tang et al. [91] in 2001 from a solution of 1-methyl-1,2,3,4,5-pentaphenylsilole. They referred to this phenomenon as aggregation-induced emission (AIE) and subsequently showed that the restriction of intramolecular rotation (RIR) in the aggregates was the main cause of AIE phenomenon. Unhindered intramolecular rotation of AIE molecules under the free state leads to efficient nonradiative decay of the corresponding excited states, making them nonemissive. In view of such interesting fluorescence behaviors, AIE phenomenon have been successfully utilized to design sensitive and selective chemosensors suitable for the detection of PPI in living cells.

Chao and Ni [92] reported a terpyridine-Zn complex **26**-Zn (Table 7) for selective nanomolar PPI detection over ATP and ADP in DMSO aqueous mixture based on AIE and ICT. Complex **26**-Zn bears a donor-acceptor (D-A) structure in which the carbazole group is the donor and the terpyridine-Zn part is the acceptor; therefore, an ICT effect was observed. In fact, terpyridine-Zn complexes bearing

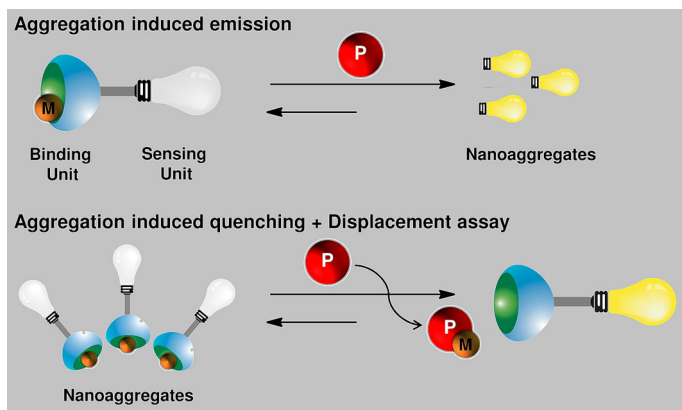
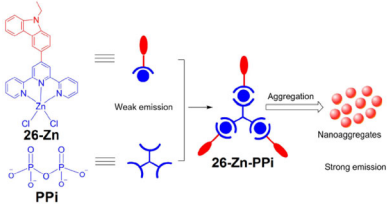
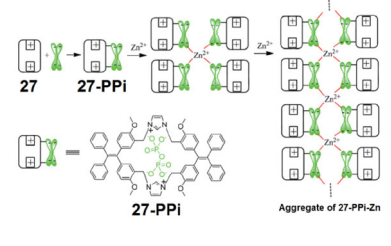
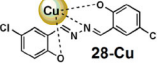
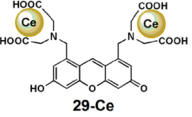


Fig. 8 Schematic overview of the sensors working in aggregation-induced emission and aggregation-induced quenching in combination with displacement assay upon binding with phosphate (*P*). *M* Metal

the D–A structure displayed different emission in solvents with various polarities, and especially weak emission was found in aqueous solution due to the strong polarity of water. When the terpyridine–Zn–PPi ensemble (3:1 binding mode) formed nanoaggregates with an average particle size of about 300 nm, as confirmed by dynamic light scattering (DLS), SEM and transmission electron microscopy, the quenching effect caused by a polar solvent, such as water, can be inhibited efficiently, leading to the strong emission at 515 nm, which is known as AIE. Other anions, including Pi, led to negligible changes for the emission of **26**–Zn but NPP induced less effects on the emission than PPI. The sensor **26**–Zn has been successfully employed for nucleus staining in living HeLa cells (Fig. 9).

A tetraphenylethylene imidazolium macrocycle **27** (Table 7) was reported to be a selective fluorescence Turn-ON sensor of PPI by Zheng et al. [93] in 2015. This positively charged macrocycle showed a maximum AIE effect in DMSO aqueous mixture, in the presence of a half eq. of Zn²⁺ with 2.4 eq. of PPI, while other common inorganic anions gave almost no response. In the presence of Zn²⁺, the UV–Vis titration of **27** with PPI was very similar to that of **27** without Zn²⁺, indicating that the metal ions did not directly interact with the macrocycle but only with the PPI. The association constant of the complex, according to a 1:1 molar ratio between **27** and PPI, as confirmed by ESI MS, was calculated to be $1.41 \times 10^4 \text{ M}^{-1}$. The crystal structure of **27** indicates that the distance between the nitrogen atoms of each imidazolium unit was approximately 5.836 Å, while the longest distance between the oxygen atoms of each phosphate unit of PPI was 5.36 Å. Therefore, the cavity of **27** is composed of two imidazolium units and is suitable for the inclusion of one molecule of PPI to form a **27**–PPI complex, driven by an electrostatic attraction. In the presence of Zn²⁺, the two component **27**–PPI complex was transformed into a five component (**27**–PPI)₄–Zn complex due to one Zn cation being coordinated by two **27**–PPI complexes. With continued coordination, an aggregate of (**27**–PPI)₄–Zn complexes formed, with the average diameter of

Table 7 Aggregation induced emission/quenching specific to inorganic pyrophosphate

Chemical structures	Fluorescence sensing properties Proposed sensing mechanism (solvent system)	Applications	Ref.
Aggregation induced emission			
	Emission ON (~ 4500-fold at 515 nm) λ_{ex} = 400 nm RIR/ICT (DMSO-10 mM HEPES, pH 7.4, 3 /7 v/v)	Nucleus staining in HeLa cells	[92]
	Emission ON (~ 25-fold at 472 nm) λ_{ex} = 347 nm RIR (water containing 0.5% DMSO)	NA	[93]
	Emission ON (~ 40-fold at 570 nm) λ_{ex} = 388 nm RIR (DMSO-10 mM Tris-HCl, pH 7.0, 2/8 v/v)	Analysis of PPI in a fetal bovine serum sample	[95]
Aggregation induced quenching			
	Emission ON (~ 318-fold at 529 nm) λ_{ex} = 500 nm AIQ/self-quenching of the xanthene fluorophore in the aggregated state (CH ₃ OH-25 mM MES, pH 6.8, 1/1 v/v)	Detection of viral infection using nucleic acid amplification reaction	[76]

λ_{ex} excitation wavelength, NA not available

aggregates being up to 2800 nm as confirmed by DLS; therefore, the strong fluorescence was probably due to a RIR mechanism [94].

Another AIE fluorescence mechanism using 5-chlorosalicylaldehyde azine **28** induced by Cu²⁺ (Table 7) followed by PPI was reported by Tong et al. [95] in 2015. The structure of salicylaldehyde azine derivatives provided the AIE characteristic, as well as the potential chelating sites for metal ions [96, 97]. Compound **28** showed a strong fluorescence in the DMSO volume fraction range of 10–50%, which was considered to be AIE fluorescence in its aggregated state. In contrast, in a high DMSO volume fraction range of 70–90%, a weak fluorescence

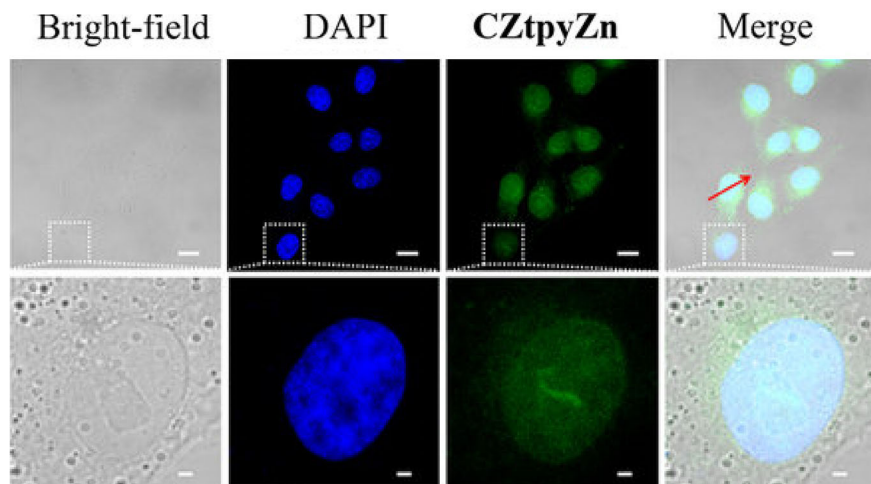


Fig. 9 Confocal fluorescence images of HeLa cells incubated with **26**-Zn (5×10^{-6} M) for 30 min and then further incubated with 4',6-diamidino-2-phenylindole (DAPI; 5×10^{-6} g mL $^{-1}$) for 10 min. The blue channel for DAPI excited at 405 nm and the green channel for **26**-Zn excited at 488 nm. Scale bar: 20 μ m. This work is licensed under a Creative Commons Attribution 4.0 International License

was observed due to the free rotation of N–N single bond in solution state. According to DLS data, the mean diameter of the fluorescent aggregates of **28** was 533.5 nm. The addition of Cu $^{2+}$ considerably reduced the size of the fluorescent aggregates to 279.4 nm, which might be due to the better solubility of the **28**–Cu complex. The addition of PPI led to the generation of fluorescent aggregates once again, with a mean size of 506.0 nm, which was close to that of **28** in the same solvent system. The fluorescence response of ADP and ATP was 25% and nearly 100%, respectively, of that of PPI. Negative charges at neutral pH for these NPPs were supposed to be responsible for their coordinating ability with Cu $^{2+}$. An application to the analysis of PPI in a protein removed from 50-fold diluted fetal bovine serum sample was also demonstrated.

On the other hand, a unique combination of displacement assay and aggregation-induced quenching (Fig. 8) was first introduced by Ojida and Wongkongkatap et al. [76] in 2014. The xanthene probe–Ce $^{3+}$ complex **29**–Ce (Table 7) was reported as a selective fluorescence sensor of PPI in methanol aqueous solution. The **29**–Ce complex forms an aggregated polymer through bridging coordination interactions between **29** and Ce $^{3+}$ ions; therefore the large fluorescence decrease of **29** upon complexation with Ce(NO $_3$) $_3$ is ascribed to self-quenching of the xanthene fluorophore in the aggregated state and the quenching effect of the coordinated Ce $^{3+}$ ions. When PPI was added to a solution of the **29**–Ce complex, its fluorescence increased drastically ($I/I_0 = 318$) upon addition of over 20 eq. PPI. ESI–MS showed that **29** mainly exists as the free ligand in the presence of 20 eq. PPI, indicating that coordination exchange occurs between **29**–Ce and PPI to form a Ce $^{3+}$ –PPI complex and to liberate the fluorescent ligand **29**. Other phosphate species, including NPP, and other oxoanions scarcely induced an increase in

fluorescence except for Pi ($I/I_0 = 28$) and uridine-5'-triphosphate ($I/I_0 = 30$). The fluorescence detection of DNA polymerase-catalyzed nucleic acid amplification by the loop-mediated isothermal amplification method for viral infection diagnosis using the **29**-Ce complex was demonstrated (Fig. 10).

3.3 Chemical Reactions

Not only molecular recognition, but the binding interaction between host and guest molecules can be based on an irreversible formation of a covalent bond. Such indicators are described as a chemodosimeter [98]. Chemodosimeters require at least two functional units, namely, the reaction site, where the host binds to the analyte covalently, and the sensing unit, which is dependent on the interaction with the analyte. The analyte reacts with the sensor to create a new molecule with different optical properties (Fig. 11). Because of their high sensitivity and selectivity, the design, synthesis, and application of chemodosimeters in luminescence bioimaging of Pi/PPi have attracted increasing attention and become an active research field.

3.3.1 Pi Sensing

Zhou et al. [99] reported the fluorescence properties of compound **30** containing an oxalate moiety linked via an ester bond to the hydroxyl group of coumarin fluorophore. The selective reaction of **30** toward Pi led to the cleavage of the ester bond and liberation of the fluorophores (Table 8). This unique Pi-induced hydrolytic reaction was effective in DMSO-HEPES buffered solutions that produce a colorimetric change associated with a 62-nm red-shift in the UV-Vis absorption maximum and up to a 780-fold enhancement in the fluorescence intensity; in contrast the addition of uridine monophosphate (UMP) and guanosine monophosphate (GMP) to solutions of **30** resulted in minor fluorescence enhancement (UMP 5.3-fold, GMP 3.6-fold), while common other anions, including NPP, cysteine, glutathione, and glutamic acid did not promote any change in emission. DFT calculations depicted the energy changes occurring in the hydrolytic reaction to be about -19.3 kJ. Mass spectrometry analysis of a mixture of **30** and 100 eq. of Pi in DMSO-HEPES buffer after stirring for 12 h contained a peak at m/z 151.08 corresponding to the cyclic diphosphate (Table 8). Fluorescence imaging studies were carried out using HeLa cells and *Caenorhabditis elegans* with the addition of 4 eq. exogenous Pi, or ATP and apyrase. A clearly detectable bright blue fluorescence was emitted, indicating the increase in endogenous Pi as a result of ATP hydrolysis catalyzed by Apyrase. Another application was performed using Sf9 adherent cells derived from *Spodoptera frugiperda* pupal ovarian tissue and treated with innexin 2 or 3 as an apoptosis inducer. Treatment of Sf9 cells with **30** and innexin 3 in the absence of Apyrase resulted in a clearly detectable fluorescent image, thereby demonstrating that innexin 3 caused dephosphorylation of Akt (protein kinase B) in hemichannel-closed cells that led to apoptosis.

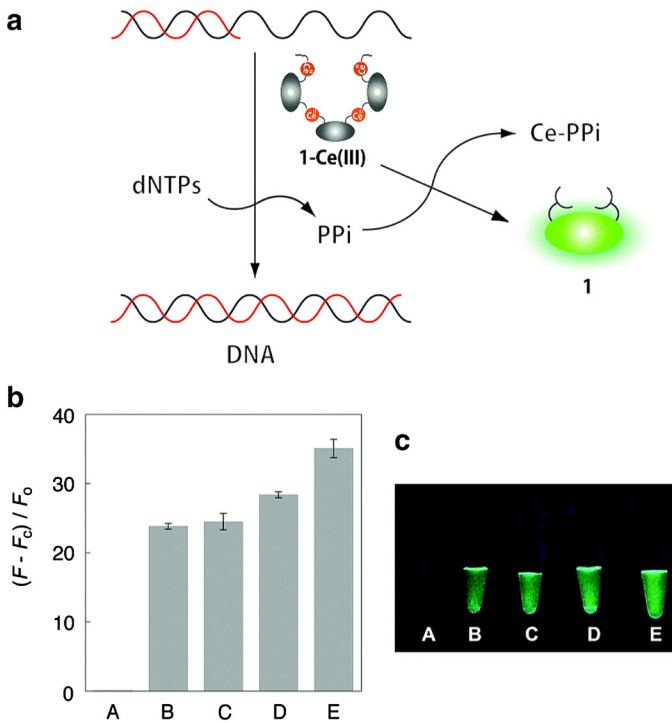


Fig. 10 **a** Mechanism of the fluorescent loop-mediated isothermal amplification (LAMP) assay using the 29-Ce complex. **b** Changes in fluorescence of the 29-Ce complex upon addition of the LAMP reaction solution. Each reaction was conducted in the presence of 0 (A), 2 (B), 20 (C), 200 (D), and 1000 (E) copies of white spot syndrome virus plasmid DNA. Conditions [29]: 5×10^{-6} M, 0.27 mM $\text{Ce}(\text{NO}_3)_3$, 25 mM MES (pH 6.8)- CH_3OH (1:1), 25 °C, $\lambda_{\text{ex}} = 500$ nm. The y-axis indicates the ratio of the fluorescence increase of each sample $[(F - F_c)/F_0]$, where F , F_c , and F_0 are the fluorescence intensity of the reaction sample, of the control reaction sample without plasmid, and of the solution of the 29-Ce³⁺ complex, respectively. **c** Photographs of solutions of the 29-Ce complex upon addition of LAMP reaction solutions. Adapted from Kittiloespaisan et al. [76] by permission of The Royal Society of Chemistry

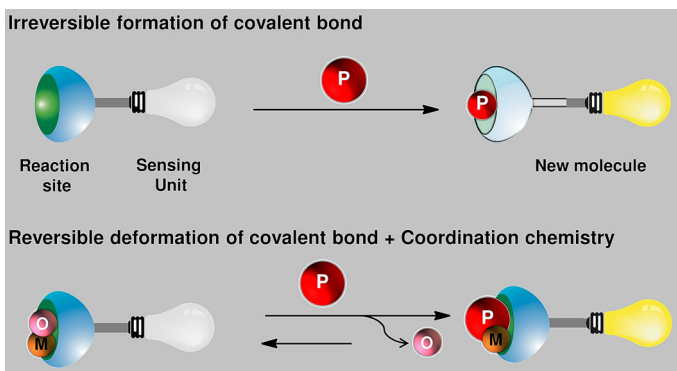
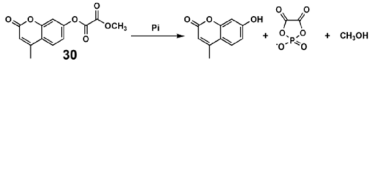
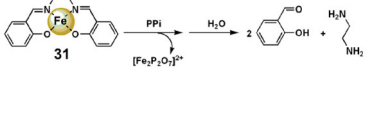
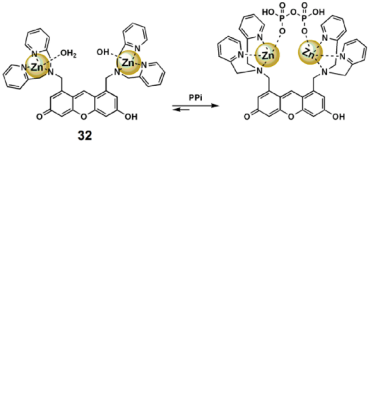


Fig. 11 Schematic overview of the reaction-based sensing mechanism. *M* Metal, *O* covalently bound oxygen, *P* phosphate

Table 8 Sensing through reactions specific to inorganic phosphate/inorganic pyrophosphate

Chemical reactions	Fluorescence sensing properties	Applications	Ref.
 <p>Reaction of compound 30 with Pi to form a fluorescent product, PPi, and CH_3OH.</p>	<p>Emission ON (~ 780-fold at 455 nm)</p> <p>$\lambda_{\text{exc}} = 385 \text{ nm}$</p> <p>NA</p> <p>(DMSO-0.02 M HEPES, pH 7.4, 9/1 v/v)</p>	<p>Bioimaging using HeLa cells and <i>C. elegans</i> treated with exogenous 4 eq. Pi or 4 eq. of ATP + apyrase</p> <p>Bioimaging of Sf9 adherent cells treated with innexin 2 or 3 with/without apyrase</p>	[99]
 <p>Reaction of compound 31 with PPi and H_2O to form salicylaldehyde and H_2N, releasing $[\text{Fe}_3\text{P}_2\text{O}_7]^{4-}$.</p>	<p>Emission ON (~ 36-fold at 500 nm)</p> <p>$\lambda_{\text{exc}} = 350 \text{ nm}$</p> <p>MLCT</p> <p>(10 mM Tris, pH 7.4)</p>	<p>Fluorescence imaging of endogenous PPi in mitochondria of HeLa cells incubated with the ANK protein inhibitor probenecid.</p>	[100]
 <p>Reaction of compound 32 with PPi to form a fluorescent product.</p>	<p>Emission ON (~ 55-fold at 523 nm)</p> <p>$\lambda_{\text{exc}} = 488 \text{ nm}$</p> <p>Binding-induced recovery of the conjugated form of the xanthene fluorophore</p> <p>(50 mM HEPES, 10 mM NaCl, 1 mM MgCl_2, pH 7.4)</p>	<p>Fluorescent staining of intracellular ATP storage in live Jurkat cells [101]</p> <p>Fluorescent assay of hydrolysis pathway of diadenosine tetraphosphate [102]</p> <p>Organelle-localized multicolor fluorescence probes useful for imaging of NPP dynamics in living cells [103]</p> <p>Detection of nucleic acid amplification reaction useful for diagnosis of viral infection [104]</p> <p>Detection of pathogenic spore-forming bacteria through the intracellular ATP pool [105]</p> <p>Visualization of red blood cell CR1-mediated ATP release [106]</p>	[101-106]

3.3.2 *PPi* Sensing

Zelder et al. [100] reported a metal disassembly strategy concurrent with reaction for imaging endogenous PPi in the mitochondria of HeLa cells by using the square pyramidal Fe^{3+} -salen complex **31** (Table 8). Non-fluorescent **31** displayed an approximately 36-fold increase in emission intensity upon the addition of PPi in aqueous solution (pH 7.4), with a saturation of the intensity at approximately 25 min. Minor increases in emission were observed following the addition of NPP and Pi , but no other anions showed any effects. UV/Vis spectroscopy suggested that the presence of PPi led to a disappearance of the MLCT band of **31**. Job plot analysis indicated a 2:1 stoichiometry for the reaction between **31** and PPi at physiological pH, and an equilibrium constant value ($\log K$) of 7.06 ± 04 was calculated. The reaction-based release of fluorescent salicylaldehyde upon

disassembly of **31** in the presence of PPI was confirmed with ESI MS, and the fluorescence properties of salicylaldehyde were compared with the reaction mixture.

A reversible covalent bond destruction leading to a change in optical properties of the sensing unit upon specific binding to the target molecule is also possible (Fig. 11). This unique sensing mechanism was first noted by Ojida and Hamachi et al. [101] and was used for an excellent design of a Turn-ON fluorescent PPI/NPP sensor. Sensor **32** comprises two DPA-Zn moieties as a binding motif for the PPI and the xanthene fluorophore as a sensing unit (Table 8). In the absence of PPI/NPP, the bridging water between the two Zn²⁺ centers attacked the ring of xanthene fluorophore breaking down a fluorescent π -conjugated ring under a wide pH range of 6–9 in 100% aqueous solution. Upon molecular recognition of PPI/NPP by the two Zn centers, the coordination geometry was modulated as the attacking water was removed to recover the fluorescent xanthene conjugated ring (Fig. 12).

It should be noted that this novel reversible mechanism is a result of the good cooperation between the chemical reaction and coordination chemistry which demonstrates a high potential for several bioanalytical applications, including fluorescent staining of intracellular ATP storage in live Jurkat cells [101], fluorescent assay of the hydrolysis pathway of diadenosine tetraphosphate [102], organelle-localized multicolor fluorescence probes useful for imaging of NPP dynamics in living cells (Fig. 13) [103], detection of nucleic acid amplification reaction useful for viral infection diagnosis [104], detection of pathogenic spore-

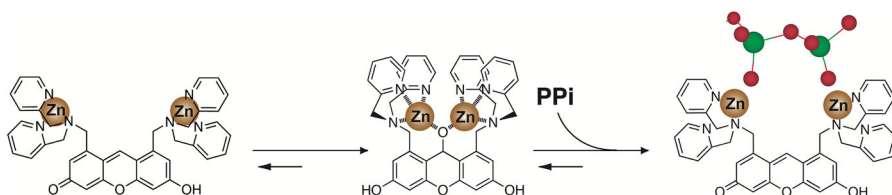


Fig. 12 Schematic illustration of a combination between chemical reaction and coordination chemistry as a reversible destruction of the covalent bond between bridging oxygen and xanthene ring results in a unique sensing mechanism of inorganic pyrophosphate (PPI)/nucleoside polyphosphate achieved by compound **32**

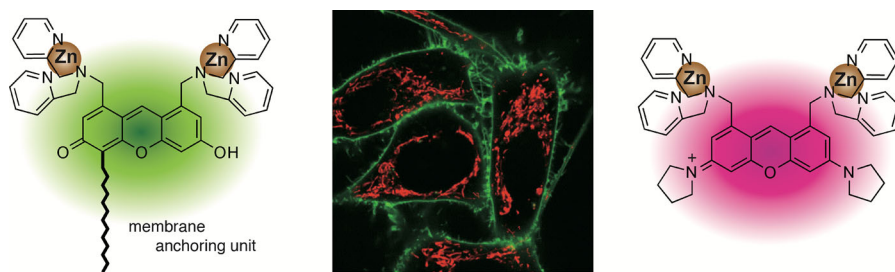


Fig. 13 Confocal fluorescence analysis of HeLa cells stained with green **32** bearing a biocompatible anchor for membrane unit and pink **32** with a positively charged pyronin ring. Reprinted with permission from Kurishita et al. [103]. Copyright 2012 American Chemical Society

forming bacteria through the intracellular ATP pool [105], and fluorescent visualization of red blood cell complement receptor 1-mediated ATP release [106].

4 Conclusion

In this review we have summarized how small molecular sensors turn their fluorescence ON or OFF in response to organophosphates, including Pi and PPi as well as potential applications. Hydrogen bonding interaction is quite useful for sensing in organic solvent where the hydration energy is weaker than the self-assemble capability between the sensor and the target molecule. Coordination chemistry provides a great advantage for selective binding of an oxoanion in a complete aqueous solution or the mixture. Several new sensing mechanisms, such as displacement assay, aggregation-induced emission, and chemical reactions enable the high sensitivity and selectivity for Pi/PPi detection. Towards this goal, new molecular design and sensing mechanisms which realize specific sensing of each phosphate species, including Pi/PPi, are urgently required. The development of a new sensing chemistry applicable to practical use is a worthy challenge for many chemists.

Acknowledgements JW is grateful to the Faculty of Science, Mahidol University and the Thailand Research Fund (IRG5980001).

References

1. Lee GJ, Marks J (2015) Intestinal phosphate transport: a therapeutic target in chronic kidney disease and beyond? *Pediatr Nephrol* 30:363–371
2. Hansen NM, Felix R, Bisaz S, Fleisch H (1976) Aggregation of hydroxyapatite crystals. *Biochim Biophys Acta* 451:549–559
3. Crook M, Swaminathan R (1996) Disorders of plasma phosphate and indications for its measurement. *Ann Clin Biochem* 33:376–396
4. Prie D, Beck L, Friedlander G, Silve C (2004) Sodium-phosphate cotransporters, nephrolithiasis and bone demineralization. *Curr Opin Nephrol Hypertens* 13:675–681
5. Knochel JP, Barcenac C, Cotton JR, Fuller TJ, Haller R, Carter NW (1978) Hypophosphatemia and rhabdomyolysis. *J Clin Invest* 62:1240–1246
6. Knochel JP (1977) The pathophysiology and clinical characteristics of severe hypophosphatemia. *Arch Intern Med* 137:203–220
7. Khoshniat S, Bourguin A, Julien M, Weiss P, Guicheux J, Beck L (2011) The emergence of phosphate as a specific signaling molecule in bone and other cell types in mammals. *Cell Mol Life Sci* 68:205–218
8. Rutecki GW, Cugino A, Jarjoura D, Kilner JF, Whittier FC (1997) Nephrologists' subjective attitudes towards end-of-life issues and the conduct of terminal care. *Clin Nephrol* 48:173–180
9. Weisinger JR, Bellorin-Font E (1998) Magnesium and phosphorus. *Lancet* 352:391–396
10. Shiber JR, Mattu A (2002) Serum phosphate abnormalities in the emergency department. *J Emerg Med* 23:395–400
11. Hruska KA, Mathew S, Lund RJ, Memon I, Saab G (2009) The pathogenesis of vascular calcification in the chronic kidney disease mineral bone disorder: the links between bone and the vasculature. *Semin Nephrol* 29:156–165
12. Kanbay M, Goldsmith D, Akcay A, Covic A (2009) Phosphate - the silent stealthy cardiorenal culprit in all stages of chronic kidney disease: a systematic review. *Blood Purif* 27:220–230
13. Hruska KA, Mathew S, Lund R, Qiu P, Pratt R (2008) Hyperphosphatemia of chronic kidney disease. *Kidney Int* 74:148–157

14. Devlin TM (2010) Textbook of biochemistry with clinical correlations, 7th edn. Wiley, New York
15. Heinonen JK (2001) Biological role of inorganic pyrophosphate, 1st edn. Kluwer, Dordrecht
16. Florence WLT (2012) Genetics and mechanisms of crystal deposition in calcium pyrophosphate deposition disease. *Curr Rheumatol Rep* 14:155–160
17. Costello JC, Rosenthal AK, Kurup IV, Masuda I, Medhora M, Ryan LM (2011) Parallel regulation of extracellular ATP and inorganic pyrophosphate: roles of growth factors, transduction modulators, and ANK. *Connect Tissue Res* 52:139–146
18. Rosenthal AK, Gohr CM, Mitton-Fitzgerald E, Lutz MK, Dubyak GR, Ryan LM (2013) The progressive ankylosis gene product ANK regulates extracellular ATP levels in primary articular chondrocytes. *Arthritis Res Ther* 15:R154
19. Rosenthal AK, Ryan LM (2016) Calcium pyrophosphate deposition disease. *N Engl J Med* 374:2575–2584
20. Chen M, Graedel TE (2016) A half-century of global phosphorus flows, stocks, production, consumption, recycling, and environmental impacts. *Glob Environ Change* 36:139–152
21. Mason CF (1991) Biology of freshwater pollution. Longman, New York
22. Hargrove AE, Nieto S, Zhang T, Sessler JL, Anslyn EV (2011) Artificial receptors for the recognition of phosphorylated molecules. *Chem Rev* 111:6603–6782
23. Hirsch AKH, Fischer FR, Diederich F (2007) Phosphate recognition in structural biology. *Angew Chem Int Ed* 46:338–352
24. Kim SK, Lee DH, Hong J-I, Yoon J (2009) Chemosensors for pyrophosphate. *Acc Chem Res* 42:23–31
25. Lee S, Yuen KKY, Jolliffe KA, Yoon J (2015) Fluorescent and colorimetric chemosensors for pyrophosphate. *Chem Soc Rev* 44:1749–1762
26. Busschaert N, Caltagirone C, Rossom WV, Gale PA (2015) Applications of supramolecular anion recognition. *Chem Rev* 115:8038–8155
27. Wu J, Liu W, Ge J, Zhang H, Wang P (2011) New sensing mechanisms for design of fluorescent chemosensors emerging in recent years. *Chem Soc Rev* 40:3483–3495
28. Ngo HT, Liu X, Jolliffe KA (2012) Anion recognition and sensing with Zn(II)-dipicolylamine complexes. *Chem Soc Rev* 41:4928–4965
29. Pak YL, Swamy KMK, Yoon J (2015) Recent progress in fluorescent imaging probes. *Sensors* 15:24374–24396
30. Yoon J, Kim SK, Singh NJ, Kim KS (2006) Imidazolium receptors for the recognition of anions. *Chem Soc Rev* 35:355–360
31. Gale PA (2006) Structural and molecular recognition studies with acyclic anion receptors. *Acc Chem Res* 39:465–475
32. Schmidtchen FP, Berger M (1997) Artificial organic host molecules for anions. *Chem Rev* 97:1609–1646
33. Marcus Y, Rashin A (1994) A simple empirical model describing the thermodynamics of hydration of ions of widely varying charges, sizes, and shapes. *Biophys Chem* 51:111–127
34. Czarnik AW (1994) Chemical communication in water using fluorescent chemosensors. *Acc Chem Res* 27:302–308
35. Chen K-H, Yang J-S, Hwang C-Y, Fang J-M (2008) Phospholipid-induced aggregation and anthracene excimer formation. *Org Lett* 10:4401–4404
36. Lee M, Moon JH, Jun EJ, Kim G, Kwon Y-U, Lee JY, Yoon J (2014) A tetranaphthoimidazolium receptor as a fluorescent chemosensor for phytate. *Chem Commun* 50:5851–5853
37. Zheng F, Guo S, Zeng F, Li J, Wu S (2014) Ratiometric fluorescent probe for alkaline phosphatase based on betaine-modified polyethylenimine via excimer/monomer conversion. *Anal Chem* 86:9873–9879
38. Kumar R, Srivastava A (2016) Anion binding-induced white light emission using a water-tolerant fluorescent molecular tweezer. *Chem Eur J* 22:3224–3229
39. Nishizawa S, Kato Y, Teramae N (1999) Fluorescence sensing of anions via intramolecular excimer formation in a pyrophosphate-induced self-assembly of a pyrene-functionalized guanidinium receptor. *J Am Chem Soc* 121:9463–9464
40. Qian X, Xiao Y, Xu Y, Guo X, Qian J, Zhu W (2010) “Alive” dyes as fluorescent sensors: fluorophore, mechanism, receptor and images in living cells. *Chem Commun* 46:6418–6436
41. Wu FY, Li Z, Guo L, Wang X, Lin MH, Zhao YF, Jiang YB (2006) A unique NH-spacer for *N*-benzamidothiourea based anion sensors. Substituent effect on anion sensing of the ICT dual fluorescent *N*-(*p*-dimethylaminobenzamido)-*N*-arylothioureas. *Org Biomol Chem* 4:624–630
42. Steed JW (2009) Coordination and organometallic compounds as anion receptors and sensors. *Chem Soc Rev* 38:506–519

43. Ojida A, Mito-oka Y, Inoue M, Hamachi I (2002) First artificial receptors and chemosensors toward phosphorylated peptide in aqueous solution. *J Am Chem Soc* 124:6256–6258
44. Ojida A, Mito-oka Y, Sada K, Hamachi I (2004) Molecular recognition and fluorescence sensing of monophosphorylated peptides in aqueous solution by bis(Zn(II)-dipicolylamine)-based artificial receptors. *J Am Chem Soc* 126:2454–2463
45. Elangannan A, Desiraju GR, Klein RA, Sadlej J, Scheiner S, Alkorta I, Clary DC, Crabtree RH, Dannenberg JJ, Hobza P, Kjaergaard HG, Legon AC, Mennucci B, Nesbitt DJ (2011) Definition of the hydrogen bond. *Pure Appl Chem* 83:1637–1641
46. S-i Kondo, Takai R (2013) Selective detection of dihydrogen phosphate anion by fluorescence change with tetraamide-based receptors bearing isoquinolyl and quinolyl moieties. *Org Lett* 15:538–541
47. Zhang D, Jiang X, Yang H, Su Z, Gao E, Martinez A, Gao G (2013) Novel benzimidazolium-urea-based macrocyclic fluorescent sensors: synthesis, ratiometric sensing of H_2PO_4^- and improvement of the anion binding performance via a synergistic binding strategy. *Chem Commun* 49:6149–6151
48. Zhang D, Jiang X, Yang H, Martinez A, Feng M, Donga Z, Gao G (2013) Acridine-based macrocyclic fluorescent sensors: self-assembly behavior characterized by crystal structures and a tunable bathochromic-shift in emission induced by H_2PO_4^- via adjusting the ring size and rigidity. *Org Biomol Chem* 11:3375–3381
49. Martí-Centelles V, Burguete MI, Galindo F, Izquierdo MA, Kumar DK, White AJP, Luis SV, Vilar R (2012) Fluorescent acridine-based receptors for H_2PO_4^- . *J Org Chem* 77:490–500
50. Gong W, Zhang Q, Wang F, Gao B, Lin Y, Ning G (2012) Selective sensing of H_2PO_4^- (Pi) driven by the assembly of anthryl pyridinium ligands. *Org Biomol Chem* 10:7578–7583
51. Caltagirone C, Bazzicalupi C, Isaia F, Light ME, Lippolis V, Montis R, Murgia S, Olivari M, Picci G (2013) A new family for bis-ureidic receptors for pyrophosphate optical sensing. *Org Biomol Chem* 11:2445–2451
52. Casula A, Bazzicalupi C, Bettoschi A, Cadoni E, Coles SJ, Horton PN, Isaia F, Lippolis V, Mapp LK, Marini GM, Montis R, Scorciapino MA, Caltagirone C (2016) Fluorescent asymmetric bis-ureas for pyrophosphate recognition in pure water. *Dalton Trans* 45:3078–3085
53. Sanchez G, Espinosa A, Curiel D, Tarraga A, Molina P (2013) Bis(carbazolyl)ureas as selective receptors for the recognition of hydrogen pyrophosphate in aqueous media. *J Org Chem* 78:9725–9737
54. Yuan Y, Gao G, Jiang ZL, You JS, Zhou ZY, Yuan DQ, Xie RG (2002) Synthesis and selective anion recognition of imidazolium cyclophanes. *Tetrahedron* 58:8993–8999
55. Bhalla V, Vij V, Kumar M, Sharma PR, Kaur T (2012) Recognition of adenosine monophosphate and H_2PO_4^- using zinc ensemble of new hexaphenylbenzene derivative: potential bioprobe and multichannel keypad system. *Org Lett* 14:1012–1015
56. Ni XL, Zeng X, Redshaw C, Yamato T (2011) Ratiometric fluorescent receptors for both Zn^{2+} and H_2PO_4^- ions based on a pyrenyl-linked triazole-modified homooxacalix[3]arene: a potential molecular traffic signal with an R-S latch logic circuit. *J Org Chem* 76:5696–5702
57. Lee HN, Swamy KMK, Kim SK, Kwon J-Y, Kim Y, Kim S-J, Yoon YJ, Yoon J (2007) Simple but effective way to sense pyrophosphate and inorganic Phosphate by fluorescence changes. *Org Lett* 9:243–246
58. Nadella S, Selvakumar PM, Suresh E, Subramanian PS, Albrecht M, Giese M, Fröhlich R (2012) Lanthanide(III) complexes of bis-semicarbazone and bis-imine-substituted phenanthroline ligands: solid-state structures, photophysical properties, and anion sensing. *Chem Eur J* 18:16784–16792
59. Ganjali MR, Hosseini M, Memari Z, Faridbod F, Norouzi P, Goldoos H, Badiei A (2011) Selective recognition of monohydrogen phosphate by fluorescence enhancement of a new cerium complex. *Anal Chim Acta* 708:107–110
60. Nadella S, Sahoo J, Subramanian PS, Sahu A, Mishra S, Albrecht M (2014) Sensing of phosphates by using luminescent Eu^{III} and Tb^{III} complexes: application to the microalgal cell *Chlorella vulgaris*. *Chem Eur J* 20:6047–6053
61. Mahapatra AK, Ali SS, Maiti K, Manna SK, Maji R, Mondal S, Uddin MdR, Mandal S, Sahoo P (2015) Aminomethylpyrene-based imino-phenols as primary fluorescence switch-on sensors for Al^{3+} in solution and in Vero cells and their complexes as secondary recognition ensembles toward pyrophosphate. *RSC Adv* 5:81203–81211
62. Kim HJ, Lee JH, Hong J-I (2011) Highly sensitive chemosensor for detection of PPI with improved detection limit. *Tetrahedron Lett* 52:4944–4946
63. Kimura E, Shiota T, Koike T, Shiro M, Kodama M (1990) A zinc(II) complex of 1,5,9-triazacyclododecane ([12]ane N_3) as a model for carbonic anhydrase. *J Am Chem Soc* 112:5805–5811

64. Kimura E, Aoki S, Koike T, Shiro M (1997) A tris(Zn^{II} – 1,4,7,10-tetraazacyclododecane) complex as a new receptor for phosphate dianions in aqueous solution. *J Am Chem Soc* 119:3068–3076
65. Bobyr E, Lassila JK, Wiersma-Koch HI, Fenn TD, Lee JJ, Nikolic-Hughes I, Hodgson KO, Rees DC, Hedman B, Herschlag D (2012) High-resolution analysis of Zn^{2+} coordination in the alkaline phosphatase superfamily by EXAFS and X-ray crystallography. *J Mol Biol* 415:102–117
66. Kim JS, Quang DT (2007) Calixarene-derived fluorescent probes. *Chem Rev* 107:3780–3799
67. Mizukami S, Nagano T, Urano Y, Odani A, Kikuchi K (2002) A fluorescent anion sensor that works in neutral aqueous solution for bioanalytical application. *J Am Chem Soc* 124:3920–3925
68. Yang C, Fu L-M, Wang Y, Zhang J-P, Wong WT, Ai X-C, Qiao YF, Zou BS, Gui L-L (2004) A highly luminescent europium complex showing visible-light-sensitized red emission: direct observation of the singlet pathway. *Angew Chem Int Ed* 43:5010–5013
69. Zhang JF, Kim S, Han JH, Lee S-J, Pradhan T, Cao QY, Lee SJ, Kang C, Kim JS (2011) Pyrophosphate-selective fluorescent chemosensor based on 1, 8-naphthalimide-DPA-Zn(II) complex and its application for cell imaging. *Org Lett* 13:5294–5297
70. Lin J-R, Chu C-J, Venkatesan P, Wu S-P (2015) Zinc(II) and pyrophosphate selective fluorescence probe and its application to living cell imaging. *Sens Actuat B* 207:563–570
71. Jiao S-Y, Li K, Xin Wang X, Huang Z, Pu L, Yu X-Q (2015) Making pyrophosphate visible: the first precipitable and real-time fluorescent sensor for pyrophosphate in aqueous solution. *Analyst* 140:174–181
72. Ojida A, Miyahara Y, Wongkongkatep J, S-i Tamaru, Sada K, Hamachi I (2006) Design of dual-emission chemosensors for ratiometric detection of ATP derivatives. *Chem Asian J* 1:555–563
73. Bhuyan M, Katayev E, Stadlbauer S, Nonaka H, Ojida A, Hamachi I, König B (2011) Rigid luminescent bis-Zinc(II)-bis-cyclen complexes for the detection of phosphate anions and non-covalent protein labeling in aqueous solution. *Eur J Org Chem* 2011 (15):2807–2817
74. Mesquita LM, André V, Esteves CV, Palmeira T, Berberan-Santos MN, Mateus P, Delgado R (2016) Dinuclear Zinc(II) macrocyclic complex as receptor for selective fluorescence sensing of pyrophosphate. *Inorg Chem* 55:2212–2219
75. Bhowmik S, Ghosh BN, Marjomäki V, Rissanen K (2014) Nanomolar pyrophosphate detection in water and in a self-assembled hydrogel of a simple terpyridine- Zn^{2+} complex. *J Am Chem Soc* 136:5543–5546
76. Kittiloespaisan E, Takashima I, Kiatpathomchai W, Wongkongkatep J, Ojida A (2014) Coordination ligand exchange of a xanthene probe-Ce(III) complex for selective fluorescence sensing of inorganic pyrophosphate. *Chem Commun* 50:2126–2128
77. Svane S, Kjeldsen F, McKee V, McKenzie CJ (2015) The selectivity of water-based pyrophosphate recognition is tuned by metal substitution in dimetallic receptors. *Dalton Trans* 44:11877–11886
78. Nguyen BT, Anslyn EV (2006) Indicator-displacement assays. *Coordin Chem Rev* 250:3118–3127
79. You L, Zha D, Anslyn EV (2015) Recent advances in supramolecular analytical chemistry using optical sensing. *Chem Rev* 115:7840–7892
80. Meng Q, Wang Y, Yang M, Zhang R, Wang R, Zhang Z (2015) A new fluorescent chemosensor for highly selective and sensitive detection of inorganic phosphate (Pi) in aqueous solution and living cells. *RSC Adv* 5:53189–53197
81. Wu J, Gao Y, Lu J, Hu J, Ju Y (2015) A steroid-coumarin conjugate for cascade recognition of copper ion and dihydrogen phosphate: microstructural features and IMPLICATION logic gate properties. *Sens Actuat B* 206:516–523
82. Wu J, Zhao X, Gao Y, Hu J, Ju Y (2015) A steroid-salen conjugate for zinc ion recognition and its applications in test-strips, living cells imaging, and cascade recognition for dihydrogen phosphate. *Sens Actuat B* 221:334–340
83. Jiao S-Y, Li K, Zhang W, Liu Y-H, Huang Z, Yu X-Q (2015) Cd(II)-terpyridine-based complex as a ratiometric fluorescent probe for pyrophosphate detection in solution and as an imaging agent in living cells. *Dalton Trans* 44:1358–1365
84. Zhu W, Huang X, Guo Z, Wu X, Yu H, Tian H (2012) A novel NIR fluorescent turn-on sensor for the detection of pyrophosphate anion in complete water system. *Chem Commun* 48:1784–1786
85. Que EL, Chang CJ (2006) A smart magnetic resonance contrast agent for selective copper sensing. *J Am Chem Soc* 128:15942–15943
86. Datta BK, Mukherjee S, Kar C, Ramesh A, Das G (2013) Zn^{2+} and pyrophosphate sensing: selective detection in physiological conditions and application in DNA-based estimation of bacterial cell numbers. *Anal Chem* 85:8369–8375

87. Qiang J, Chang C, Zhu Z, Wei T, Yu W, Wang F, Yin J, Wang Y, Zhang W, Xie J, Chen X (2016) A dinuclear-copper(II) complex-based sensor for pyrophosphate and its applications to detecting pyrophosphatase activity and monitoring polymerase chain reaction. *Sens Actuat B* 233:591–598
88. Butler SJ, Jolliffe KA (2012) Selective pyrophosphate recognition by cyclic peptide receptors in physiological saline. *Chem Asian J* 7:2621–2628
89. Hanshaw RG, Hilkert SM, Jiang H, Smith BD (2004) An indicator displacement system for fluorescent detection of phosphate oxyanions under physiological conditions. *Tetrahedron Lett* 45:8721–8724
90. McDonough MJ, Reynolds AJ, Lee WYG, Jolliffe KA (2006) Selective recognition of pyrophosphate in water using a backbone modified cyclic peptide receptor. *Chem Commun* 2006: 2971–2973. doi: [10.1039/B606917G](https://doi.org/10.1039/B606917G)
91. Luo J, Xie Z, Lam JWY, Cheng L, Chen H, Qiu C, Kwok HS, Zhan X, Liu Y, Zhu D, Tang BZ (2001) Aggregation-induced emission of 1-methyl-1,2,3,4,5-pentaphenylsilole. *Chem Commun* 2001:1740–1741. doi: [10.1039/B105159H](https://doi.org/10.1039/B105159H)
92. Chao D, Ni S (2016) Nanomolar pyrophosphate detection and nucleus staining in living cells with simple terpyridine–Zn(II) complexes. *Sci Rep* 6:26477
93. Wang J-H, Xiong J-B, Zhang X, Song S, Zhu Z-H, Zheng Y-S (2015) Tetraphenylethylene imidazolium macrocycle: synthesis and selective fluorescence turn-on sensing of pyrophosphate anions. *RSC Adv* 5:60096–60100
94. Yan X, Wang M, Cook TR, Zhang M, Saha ML, Zhou Z, Li X, Huang F, Stang PJ (2016) Light-emitting superstructures with anion effect: coordination-driven self-assembly of pure tetraphenylethylene metallacycles and metallacages. *J Am Chem Soc* 138:4580–4588
95. Liu H, Wei R, Xiang Y, Tong A (2015) Fluorescence turn-on detection of pyrophosphate based on aggregation-induced emission property of 5-chlorosalicylaldehyde azine. *Anal Methods* 7:753–758
96. Tang W, Xiang Y, Tong A (2009) Salicylaldehyde azines as fluorophores of aggregation-induced emission enhancement characteristics. *J Org Chem* 74:2163–2166
97. Chen X, Yamaguchi A, Namekawa M, Kamijo T, Teramae N, Tong A (2011) Functionalization of mesoporous silica membrane with a Schiff base fluorophore for Cu(II) ion sensing. *Anal Chim Acta* 696:94–100
98. Yang Y, Zhao Q, Feng W, Li F (2013) Luminescent chemodosimeters for bioimaging. *Chem Rev* 113:192–270
99. Guo LE, Zhang JF, Liu XY, Zhang LM, Zhang HL, Chen JH, Xie XG, Zhou Y, Luo K, Yoon J (2015) Phosphate ion targeted colorimetric and fluorescent probe and its use to monitor endogenous phosphate ion in a hemichannel-closed cell. *Anal Chem* 87:1196–1201
100. Kumari N, Huang H, Chao H, Gasser G, Zelder F (2016) A disassembly strategy for imaging endogenous pyrophosphate in mitochondria by using an Fe^{III}–salen complex. *ChemBioChem* 17:1211–1215
101. Ojida A, Takashima I, Kohira T, Nonaka H, Hamachi I (2008) Turn-on fluorescence sensing of nucleoside polyphosphates using a xanthene-based Zn(II) complex chemosensor. *J Am Chem Soc* 130:12095–12101
102. Kohira T, Takashima I, Nonaka H, Ojida A, Hamachi I (2008) Real-time off/on-mode fluorescence assay for enzyme reactions involving nucleoside polyphosphates by use of a xanthene Zn^{II}-Dpa chemosensor. *Chem Lett* 37:1164–1165
103. Kurishita Y, Kohira T, Ojida A, Hamachi I (2012) Organelle-localizable fluorescent chemosensors for site-specific multicolor imaging of nucleoside polyphosphate dynamics in living cells. *J Am Chem Soc* 134:18779–18789
104. Kittiloepsaisan E, Ojida A, Hamachi I, Seetang-Nun Y, Kiatpathomchai W, Wongkongkatep J (2012) Label-free fluorescent detection of loop-mediated isothermal amplification of nucleic acid using pyrophosphate-selective xanthene-based Zn(II)-coordination chemosensor. *Chem Lett* 41:1666–1668
105. Tiposoth P, Khamsakhon S, Ketsub N, Pongtharangkul T, Takashima I, Ojida A, Hamachi I, Wongkongkatep J (2015) Rapid and quantitative fluorescence detection of pathogenic spore-forming bacteria using a xanthene-Zn(II) complex chemosensor. *Sens Actuat B* 209:606–612
106. Melhorn MI, Brodsky AS, Estanislau J, Khoory JA, Illigens B, Hamachi I, Kurishita Y, Fraser AD, Nicholson-Weller A, Dolmatova E, Duffy HS, Ghiran IC (2013) CR1-mediated ATP release by human red blood cells promotes CR1 clustering and modulates the immune transfer process. *J Biol Chem* 288:31139–31153